Generation of Reactive Oily Bubbles by Microfluidics and Their Applications

by

Hanrui Zheng

A thesis submitted in partial fulfillment of the requirements for the degree of

Master of Science

in

Chemical Engineering

Department of Chemical and Materials Engineering

University of Alberta

Abstract

In this study, we present a new application of droplet microfluidics in the field of mineral flotation with reactive oily microbubbles (Gas-in-Oil-in-Water Emulsion). Different designs of devices were studied. Different flow regimes were found at different flowrate ratios. We found the condition to generate the oily bubbles with the least amount of oil usage and strong robustness against the fluctuation of flowrates. Under this condition, a relation is found between the size of the bubbles and the flowrate ratios. Reactive oily bubbles with collectors in oil phase were prepared using glass microfluidic devices. Thousands of oily bubbles of around 200 μm were collected per minute and used for mineral flotation. With microflotation test, oily bubbles were seen with particles attached. With in-device mixing, more particles attached onto one oily bubble. This technique would improve the collection efficiency of the fine mineral particles by stronger attractions and higher collision efficiency.

Acknowledgement

I would like to thank to all persons who have supported me during the course of my master thesis. In particular I would like to acknowledge to:

Prof. Qingxia Liu and Prof. Neda Nazemifard for their guidance along the research project.

Bo Liu, Vu Truong and other members in reactive oily bubble projects for the help along my project.

Kiarash Keshmiri for his guidance into the details of microfabrication.

All others in Liu's research group and Nazemifard's research group for their kindly support and wonderful advice.

Carl Corbett, James Skwarok, Laurie Kachmaryk, and Jie Ru for helping me with my device setup and following technical support.

Aaron Hryciw, Stephanie Bozic, Aditi Ganji, and Scott Munro from nanoFAB for their training and technical support for working in the cleanroom.

Natural Science and Engineering Research Council of Canada (NSERC) and the Canadian Centre for Clean Carbon and Mineral Processing Technologies (CMPT) for their financial support.

At last but not least, I would like to thank my parents, for their encouragement and support from start to current.

Contents

List of Figures

List of Tables

NOMENCLATURE

Q_G	gas phase flowrate
Q_O	oil phase flowrate
Q_W	water phase flowrate
G	gas phase
O	oil phase
W	water phase
L	liquid phase
CV	coefficient of variation
DD	dodecane
DDA	dodecyl amine
HDDA	1,6-hexanediol diacrylate
HPa	palmitic acid
HLB	hydrophilic-lipophilic balance
KDX	potassium dodecyl xanthate
LSCM	laser scanning confocal microscopy
OA	oleic acid
PDMS	polydimethylsiloxane
REE	rare earth elements
SEM	scanning electron microscopy
Re	Reynolds number
ρ	density
u	velocity
d	diameter
μ	viscosity
Ca	Capillary number
γ, σ	surface tension/interfacial tension
P	flotation probability
P_c	collision probability
P_a	attachment probability
P_d	detachment probability
d_p	diameter of particle
d_b	diameter of bubble

1 Introduction

Froth flotation is a commonly used mineral extraction process utilizing the air bubbles to separate the valuable minerals from gangue.[1,2] In the column, when the rising air bubble passing through the slurry, the hydrophobic particles attach to the bubble and rise to the top, while the hydrophilic ones are left in the slurry as the tailings. Hence, the separation between the valuables and gangues can be achieved by tuning the hydrophobicity of the particles. The probability (P) of a particle being collected by a bubble in a flotation cell can be calculated by:[1,3]

$$P = P_c P_a (1 - P_d) \tag{1}$$

in which P_c is the probability of bubble particle collision, P_a is the probability of attachment, P_d is the probability of detachment. So, in order to increase the overall probability, we can increase P_c, P_a, or decrease P_d. Recently more study focusing on the low recovery of fine particles (< 50 μm), which is mainly due to the low collision probability according the following equation:[1,4]

$$P_c = A \left(\frac{d_p}{d_b} \right)^n \tag{2}$$

in which d_p is the diameter of the particle, and d_b is the diameter of the bubble, and A and n are parameters that vary for different flow regimes, can be found in Table 1.1. Re in the table, the Reynolds number, is define as:

$$Re = \frac{\rho u d_{equ}}{\mu} \tag{3}$$

where ρ is density of the fluid, u is the velocity of the fluid, d_{equ} is the equivalent diameter, and μ is the viscosity of the fluid. The poor behavior of fine particles in bubble/particle attachment can also be reflected in the low recovery rate. It is experimentally evident that the recovery of the conventional flotation highly depends on the particle diameter.[5] The good

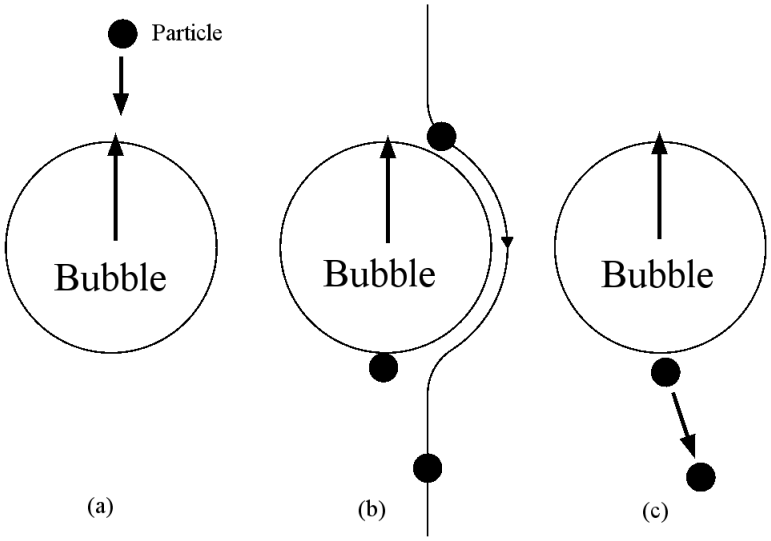

Figure 1.1: Schematic diagram of three micro-processes in flotation. (a) collision, (b) attachment, (c) detachment. This figure is re-plotted according to Tao's work.[3]

recovery rate can be obtained from particle size range from 50 μm to 250 μm;[3] however, it drops rapidly from the particle size 50 μm to about 10 μm.[6] The low collection of fine particles could be explained by the small particle volume resulting in a lack of particle/bubble collision probability. Moreover, the fine particles are tendentious to be caught in streamlines created by rising bubble, rather than to rupture the liquid film between bubble and particle (low P_c).[5,7]

To increase the collision probability, researchers reported techniques such as oil-assisted flotation, carrier flotation,[8] flocculation,[9,10] cavitation,[11] dissolved air flotation. All these methods are add-on techniques to the current flotation methods, which use some medium, such as oil, air and polymer, to form a larger floc which is easily captured by the conventional big air bubbles.

Increasing the recovery of fine particles can also be achieved by increasing the probability of attachment. P_a is affected by the hydrodynamic like P_c, but mostly by the surfaces involved.[12] Increasing P_a can be achieved by swapping the air bubbles by reactive oily bubbles. Reactive oily bubbles are air bubbles surrounded by a layer of oil containing collectors. By loading

Table 1.1: Values of A and n for different flow regimes. Re represents Reynolds number.[12]

Flow conditions	A	n
Stokes	3/2	2
Intermediate I	$\left[\frac{3}{2}+\frac{4Re^{0.72}}{15}\right]$	2
Intermediate II	$\frac{3}{2}\left[1+\frac{(3/16)Re}{1+0.249Re^{0.56}}\right]$	2
Potential	3	1

the collectors onto the carrier, the interaction between carrier and the particle is chemical interaction rather than the hydrophobic interaction in conventional method.[13] Oily bubbles attain a much higher contact angle than air bubbles, ensuring a strong collecting power, favorably for floating both coarse and fine particles. Also with no presence of collector in aqueous phase, undesired synergetic interaction can be avoided.

In the area of emulsion, reactive oily bubbles are known as Gas-in-Oil-in-Water (G/O/W) double emulsion. These double emulsions are not easily generated by sparging which is commonly used in mineral flotation. However, by utilizing microfluidics, they can be easily fabricated and tuned. Emulsion generation is a very common application of microfluidics mostly for the use within area of cosmetics, pharmaceutical, and biological industries. With the precise control of flowrate for each phase, the size and amount of these emulsions can be adjusted.

2 Objectives

The aims of this study are:

to optimize the design of the devices for reactive oily bubbles generation;

to generate reactive oily bubbles in glass microfluidic devices;

to study the effect of geometry of the channels and flowrates of phases on the flow patterns and the size of the oily bubbles;

to study the interaction between the reactive oily bubbles and mineral particles.

3 Literature Review

3.1 Mineral Flotation

Froth flotation is frequently employed for separations of solids encountered particularly in the primary mineral and chemical industries. Materials mined from any deposit within the earth's crust usually represent a highly heterogeneous mixture of solidified phases: these are mostly crystalline and represent various minerals. Occasionally. they are noncrystalline (amorphous) such as, for example, coal. glasses, resins, and opal. Crushing and grinding operations are employed to free the individual phases from their neighbors, that is, to liberate the mineral species and, occasionally, to reduce the size of solids to the range suitable for the intended separation technique. Once mineral species are liberated, an economic recovery of the valuable component(s) contained in the original mixture depends greatly on the application of the most appropriate separation or concentration process.

Of the surface properties, flotation and spherical agglomeration exploit two, surface energy and surface potential. At constant temperature, any differences in these two parameters exhibited by various minerals can be used if the solids are contacted with either two immiscible liquids, such as oil and water, or with two fluid phases, that is, a liquid and a gas. The differences in interfacial tensions lead to a preferential nonwetting of some minerals by water. This differentiation enables the hydrophobic solids to be separated in a froth if the hydrophobic solids are allowed to contact air bubbles as in froth flotation, or, alternatively, if an oil is employed as in oil flotation or in spherical agglomeration, the hydrophobic solid is collected in the oil phase.

Separation processes exploiting the surface characteristics of solids differ from all other solid/solid separation processes in the relative ease of adjusting and controlling the respective interfacial tensions and surface charges. This possibility of varying the relative properties of different interfaces contained in the system makes the froth flotation and spherical agglom-

eration processes more versatile and universal than any other industrial separation process. The physical parameters being exploited in the other separation techniques, e.g., specific gravity, magnetic susceptibility, etc., cannot be changed easily.

The surface properties of different solids are controlled by different classes of reagents, each with a specific function.

The reagents, which are used to make the mineral surface hydrophobic are called collectors and are a class of surfactants. They act by interacting at the mineral surface by adsorption or by chemical reaction. The specific compound used depends upon the nature of the mineral, chemistry of the flotation pulp and several other chemical factors.

In froth flotation, an addition of another surfactant, acting as frother is usually needed. The basic function of the frother is to produce a swarm of air bubbles, which remain sufficiently stable for the hydrophobic mineral particles to be captured by them. When the pulp within the cell becomes adequately aerated, the hydrophobic solid particles attach to air bubbles and are buoyed by them to the surface of the pulp.

In addition to chemical reagent control, the overall process of selective separation by froth flotation depends on many other factors, such as, for example, the physical and the mechanical features of thinning of liquid films, the hydrodynamics of solid-in-water slurries, the kinetics of chemical reactions and of physical processes such as wetting, and the attachment of solid and fluid phases.

3.2 Concept of Oily Bubbles

As presented in Figure 3.1, reactive oily bubbles are air bubbles with a coating of oil layer. This oil layer with surfactant presented helps to stabilize the emulsion. Instead of adding collectors into the slurry, the water phase, collectors are added to oil phase in the case of reactive oily bubbles. The interactions between the reactive oily bubbles and the minerals are chemical bonding, which is different as the hydrophobic affect happening between air bubble

and hydrophobized mineral particles. This gives stronger interactions between the carrier and the minerals, which lower the water film rupture time, hence, increase the attachment probability. With the viscous oil connecting between air and particles, the probability of detachment decreases. The distinction of reactive oily bubble technology with other flotation practices is shown in Figure 3.2. In conventional air flotation, as in Figure 3.2a, the collectors are in the slurry, attaching onto the mineral particles and modifying the surface hydrophobicity. In emulsion flotation as in Figure 3.2b, adding the collectors into the oil droplets enhancing the flotation recovery. However, dissolving collectors into a large quantity of oil in emulsion flotation incurs not only the use of an excessive amount of oil, but also a large amount of collectors to be added, encouraging the transfer of collecotrs from the oil phase to the aqueous phase. In the conventional oily bubble flotation as shown in Figure 3.2c, although only small amount of oil is required, the addition of the collector into the aqueous phase suffers all other drawbacks incurred in emulsion flotation except that only a small amount of oil is needed in this case. In contrast, reactive oily bubble flotation as shown in Figure 3.2d integrates valuable attributes of oily bubble flotation and emulsion flotation with an added advantage of small amount of collector addition.

Compared with the conventional practice in oil flotation by adding a collector in aqueous phase, dissolving collectors in oil phase in reactive oily bubbles offers the following advantages:[13]

(i) elimination of the presence of collectors in aqueous phase, thereby minimizing undesired activation of gangue particles;

(ii) reduction in the actual amount of collect required by minimizing the distribution of collectors in aqueous phase and their adsorption on undesired solids;

(iii) avoiding unnecessary synergetic interaction between the collector, frother and other chemicals present in the slurry;

(iv) a higher localized concentration of collectors at the oil/water interface, providing a

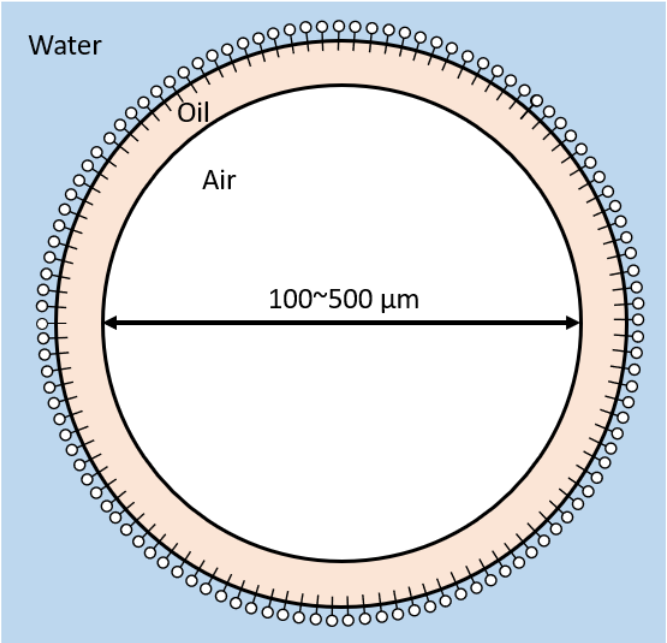

Figure 3.1: Schematic of a reactive oily bubble. The head and tail structure on the interface between water and oil phase are collectors. They also behave as surfactant stabilizing the emulsion.

stronger collecting power;

(v) only the targeted particles will be captured by the reactive oily bubbles by specific chemical interactions of collectors with active sites on the target minerals, offering a better selectivity.

Reactive oily bubbles can be used in fine particles mineral flotation in two directions: as a carrier and as an enhancer. For the carrier direction, oily bubbles replace the air bubbles as the carrier. Larger (>100 µm) oily bubbles were generated. With the advantages mentioned before, the fine particles are more likely to be floated with reactive oily bubbles. For the enhancer direction, oily bubbles were added as micrometer or submicrometer size. Their main purpose is to agglomerate the fine particles. When the oily bubbles attached onto the particles, the oil layer would be more likely to spread on the particle surface because of the low oil contact angle on the particles. Then the complex is more likely to attract other

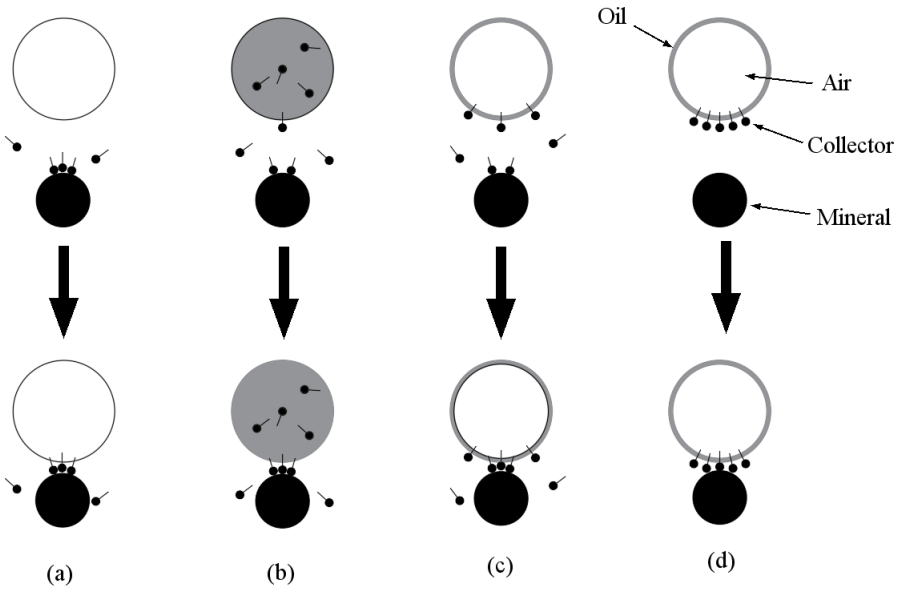

Figure 3.2: Reactive oily bubble flotation in comparison with existing flotation systems.[13] (a) conventional air flotation; (b) emulsion flotation in which oil droplets are use to life minerals but collectors are added in bulk oil to enhance collector distribution; (c) oily bubble flotation using air bubble containing a thin oil film to lift the minerals with collectors being added in the slurry; (d) the same as in (c) except that the collectors are added in oil phase to reduce collector consumption and minimize unwanted activation. Reprinted with permission from Elsevier.

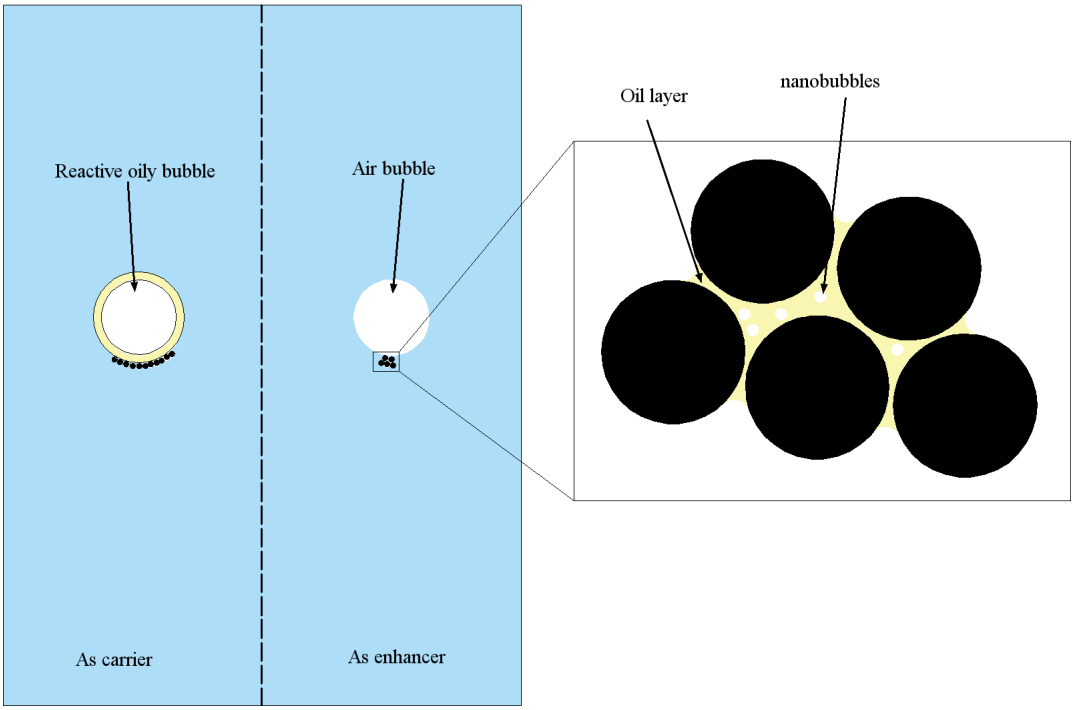

Figure 3.3: Schematic of different roles of reactive oily bubbles in mineral flotation. As the carrier, reactive oily bubbles attract fine particles and float to the froth level. While as the enhancer, reactive oily bubbles agglomerate fine particles and the agglomerates attaches to the air bubbles and float to the froth level. Light yellow represents oil, light blue represents water, white represents air, and black represents mineral particles.

particles and forms an agglomeration. The agglomerates of a larger apparent size are more favourable to attach to flotation size air bubbles, thus enhancing fine particle flotation. The two directions are shown in Figure 3.3.

All previous examples of generation of reactive oily bubbles are by flowing air through a fritted disk. Another method was proposed by Chen and others.[14] They fabricated a Janus membrane, whose one side is hydrophobic while the other side is hydrophilic. With a setup shown in Figure 3.4, they successfully fabricated G/O/W emulsions. Comparing to the use of fritted disk in other examples, membrane presents smaller holes, thus smaller

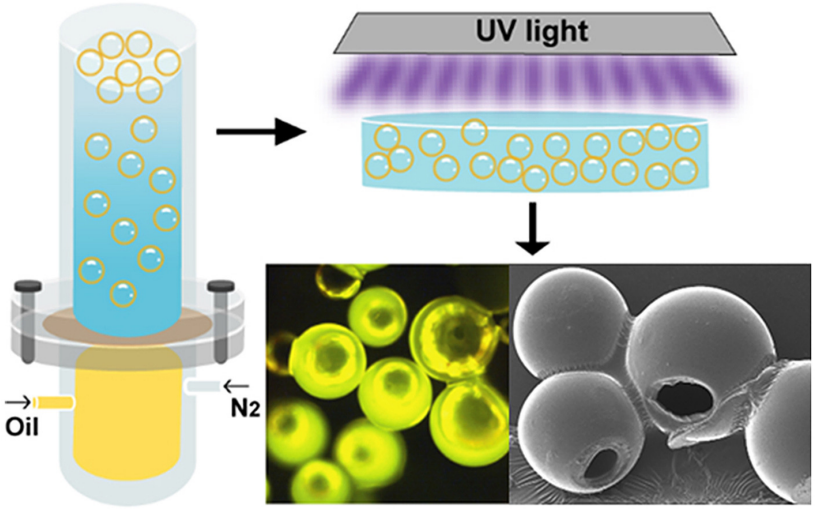

Figure 3.4: Schematic illustration of generating hollow microspheres through Janus membrane emulsification.[14] Reprinted with permission from Elsevier.

bubbles. Compared to conventional hydrophobic membrane, this Janus membrane produce even smaller emulsions because of its hydrophilic side facing to the water phase. To prove the concept, they added monomer and photoinitiator into the oil phase. After the emulsions were generated, they were exposed to UV light for 30 seconds for the monomer to polymerize. Helium ion microscope images are shown in Figure 3.4.

The reactive oily nanobubbles can be generated by high-shear mixing. By introducing gas-saturated oil-present water into the high shear mixing chamber, large amount of oil droplets, air bubbles, and oily bubbles were formed in the process. Mixing this solution with slurry containing fine particles, larger particle size distribution was observed. The oily-bubble-agglomerated slurry was also tested for a Hallimond tube flotation. Significant improvement on the recovery of the minerals was observed.

3.3 Oily Bubble Flotation

The concept of oily-bubble flotation were introduced by Liu et al. in 2002.[13] They performed the flotation on sphalerite (ZnS), galena (PbS) and silica (SiO_2) with a variety of collectors,

such as palmitic acid (HPa), potassium dodecyl xanthate (KDX), and dodecyl amine (DDA), in kerosene as the oil layer of reactive oily bubbles. They tested the contact angles of oily bubbles containing different collectors on mineral surfaces as a method to explain the flotation results which are shown in Figure 3.5. For DDA, the contact angles are very similar for ZnS and SiO_2 for most of pH values. This resulted a very similar flotation recovery for both minerals. For the presence of HPa, the contact angle and recovery of silica are both zero for all pH values. In contrast, sphalerite shows a small contact angle of 50° at acidic environment which translate to a low recovery of around 35% in the flotation test. Much better than the previous collectors, KDX shows a promising high contact angle and 100% recovery for galena, and a 90° and around 50% recovery for sphalerite at tenth of concentration of collectors comparing to the other collectors. With the collector being added into the oil phase rather than water phase, the chemical and electrokinetic properties of the reactive oily bubbles can be fine-tuned to suit desired objectives.

Wallwork et al. also apply the oily bubble technique on the recovery of bitumen in 2003.[15] They generated air bubbles with kerosene layers by condensing of mixture of evaporated kerosene and air. The study showed the addition of kerosene was beneficial for bitumen recovery in poor processing ores, an increase from around 10% to 98% for Suncor's oxidized ores. Later they conducted contact angle measurements and induction timer measurements on bitumen-coated surfaces.[16] They summarized that the increasing in recovery by oily bubbles is through increasing spreading of three-phase contact lines shown as much lower induction time of oily bubbles on bitumen than air bubbles.

Zhou et al. presented the study of use of reactive oily bubbles on selective floating apatite from dolomite and quartz in 2015.[17] Compared to Liu's work, this study focused on the oxide mineral flotation. The collector used in this case was fatty acid, which is a commercially available collector comparing to the synthesized long chain xanthate used in oily bubble sulfide flotation. The solubility of fatty acid in water is quite low, requiring higher temperature

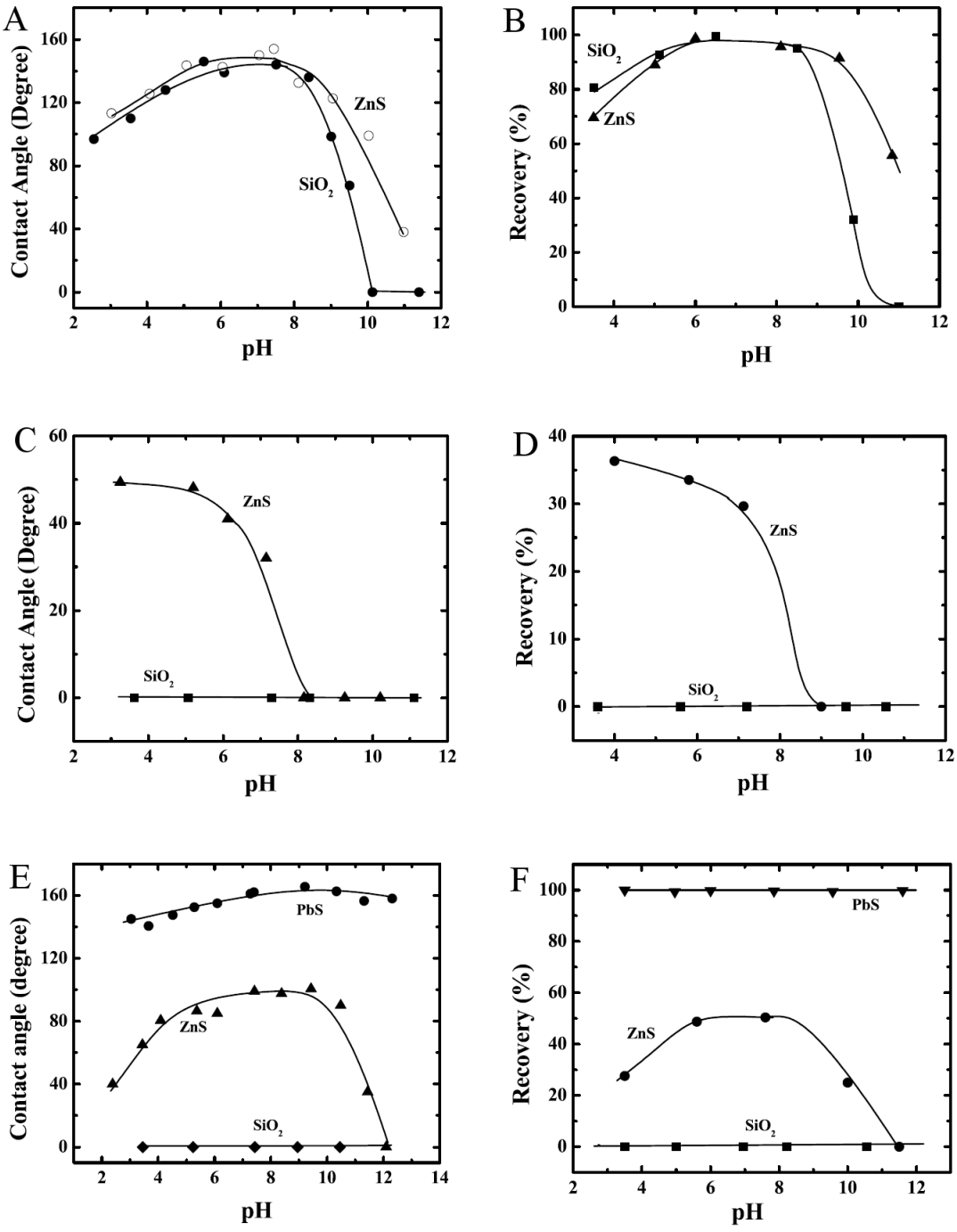

Figure 3.5: (A, C, E) Contact angles of oily bubbles on mineral surfaces and (B, D, F) flotation recovery of single minerals using reactive oily bubbles containing (A, B) 0.5 mM dodecyl amine (DDA), (C, D) 0.5 mM palmitic acid (HPa), (E, F) 0.05 mM potassium dodecyl xanthate in kerosene as a function of pH.[13] Reprinted with permission from Elsevier.

for dissolution. Therefore, the presence of collector in oil phase is more favorable than in water phase. They conducted induction timer to compare the effectiveness between reactive oily bubbles and air bubbles. The induction time of apatite attaching to reactive oily bubble (<10 ms) is much less than to air bubbles in the presence of fatty acid in water phase (30 ms). This finding suggested that the reactive oily bubble would be more effective than the conventional methods. In term of selectivity for the application of the reactive oily bubble, the induction time of apatite attaching to reactive oily bubble at pH 6 (<10 ms) is much smaller than the case of dolomite (250 ms) and quartz (>10 s). However, with the induction time in the order of 250 ms, the dolomite still can be floated. The depressant is added to the system to separate apatite from dolomite.

They also applied the same method on collophane flotation later.[18] A shorter induction time and higher recovery both showed the superiority of reactive oily bubble technique over the conventional bubble flotation in collophane flotation.

3.4 Forced Flow Flotation

The StackCell technology, developed by Eriez, provides a feasible option.[19] They decoupled the particle-bubble contacting zone from the phase separation process. The slurry and low-pressure air are feed to the contacting zone and with high shear forces, small bubbles were created, and collisions occurred. Once the slurry is discharged into the outer tank, the phase separation takes place between the froth and pulp. With such kind of technology, the general size of the tank can be made smaller, and the fine particle/bubble collision efficiency is largely improved.

3.5 Microfluidics

Microfluidics is a branch of chemical engineering that studies the design, fabrication, and operation of systems of microscopic channels that conduct fluids. Comparing to standard fluidic systems, the microfluidic channels compose at least one dimension of several to hundreds of micrometers. With this property, the flowrate inside the microchannel is usually quite low compared to conventional ones. This results a viscous force dominated system, in laminar flow regime. the microfluidics provide a simple ideal environment to study complicated matters. With the aid of lithography, complicated design can be printed onto the devices, and more controllable systems were fabricated.

3.6 Emulsion Generation by Microfluidics

At the beginning of this century, Thorsen et al.[20] demonstrated the use of a simple microfluidic device for the formation of monodisperse droplets. This report opened a completely new wave of interest in microfluidic systems that operate the flow of immiscible fluids. The use of micron-scale capillaries for construction of devices that generate monodisperse droplets[21] were know earlier. However, the report by Thorsen et al.[20] was still critical to the establishment of the new field of on-device droplet microfluidics. The fact that it was possible to control the flow of immiscible liquids with a similar fidelity as that possible for the flow of simple liquids[22] was not trivial. The ability to form monodisperse droplets in microfluidic systems, and to control virtually all the parameters of the process of formation, that is, the volume and distribution of volumes of the droplets, and the frequency of their formation, forms the basis for a number of potential applications. These applications can be divided into two general classes. The first is comprised of preparatory techniques for the formulation of new materials for the pharmaceutical, cosmetic, and food industries. The second encompasses systems for analytical and synthetic chemistry performed within individual microdroplets.

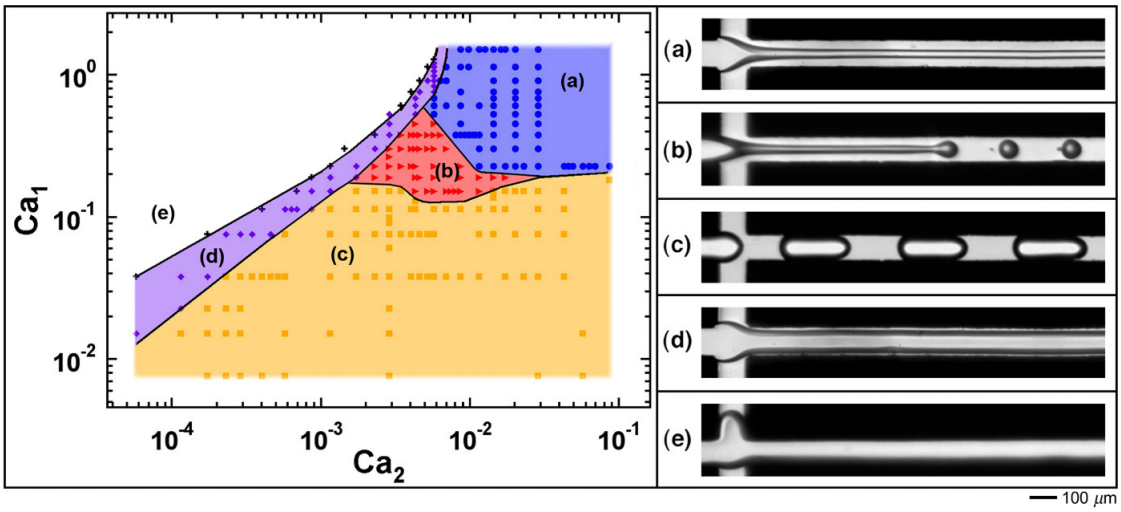

Figure 3.6: Typical capillary number-based flow map with flow patterns: (a) threading (circle), (b) jetting (triangle), (c) dripping (square), (d) tubing (diamond), (e) viscous displacement (cross).[23] Ca_1 is the capillary number of fluid 1, Glycerol, and Ca_1 is the capillary number of fluid 2, PDMS oil. Reprinted with permission from American Institute of Physics .

Cubaud and Mason studied the formation and evolution of threads containing more viscous liquids surrounded by less viscous, immiscible liquids through hydrodynamic focusing in square microchannels. Five characteristic regimes of flow behavior were defined: threading, jetting, dripping, tubing and displacement, which can be found in a flow map as shown in Figure 3.6. This study provided us with a general direction of presenting flow maps and how the flow regimes are related to capillary numbers. The capillary number is calculated by:

$$Ca = \frac{\mu u}{\sigma} \tag{4}$$

where μ is the viscosity of the continuous phase, u is the velocity of the continuous phase, and σ is the interfacial tension between phases.

3.7 Double Emlsion in Microfluidics

The most impressive use of the microfluidic control of flow in formation of droplets is exhibited in the methods of formation of multiple emulsions. Microfluidic networks of channels and the flow of fluids in these networks can be engineered to produce multiple droplets with control over practically all structural characteristics, including the number and character of the shells, and of the droplets containing within the core. The first report of the use of a microfluidic system for formation of multiple emulsions was published by Okushima and others in 2004.[24] The technique used a sequence of two T-junctions and a sophisticated control of the surface chemistry of the channels. The first T-junction is hydrophobic, including the inlet channel and the outlet from the junction. Hydrophobic character of the walls makes it possible to form aqueous dropelts in a continuous oil phase. The network of channels was designed in such a way as to have the outlet of the first T-junction become the inlet of the fluid to be dispersed in the second junction. In this second junction, the hydrophobic channel guidied the emulsion of aqueous drops in an organic continuous fluid into a perpendicular, hydrophilic channel, which supplied the outmost continuous aqueous phase. In this configuration the stream of the W-O emulsion broke in the second junction to form W-O-W droplets. They obeseved that it is possible to control the number of the aqueous dropelts contained in the larger organic droplet simply by adjusting the frequency of breakup at the first and the second junction. Similarly tuning of the rates of flow of the each of the three phases allowed for some freedom in independent tuning of the volume fraction of the inner aqueous phase in the organic shell.

In 2005, Nie et al. reported a detailed study of formation of multiple droplets in a planar flow focusing system,[25] which included the central channel that delivered the inner liquid, two, adjacent to the inner one, channels that delivered the liquid to continuous liquid. The inlet channels all terminated at the same distance upstream of the orifice. The device was fabricated in poly urethane, which favored wetting by the outermost, continuous, aqueous

phase. The inner phase comprised silicone oil that was immiscible with monomer solutions constituting the shell fluid. They found that in this simple geometry, the hydrodynamic forces were enough to engulf the inner silicone oil in the solution of monomer. These two liquids formed a centric stream that, in the orifice, broke into multiple droplets. They constructed a detailed diagram of the architectures of the droplets, attainable via appropriate tuning of the rates of flow of the three immiscible fluids. The diagram as shown in Figure 3.7, can be rationalized via the observations made that: (i) the diameter of each of the jets (inner and outer) can be very well approximated via conservation of mass, and (ii) that these jets breakup via the Rayleigh-Plateau instability with the diameter of the droplets being closely related to the wavelength of the fastest mode of collapse of an unstable column of liquid. The conservation of mass can be applied via an approximation that both jets flow at the speed of the continuous liquid. This former speed can be easily estimated from the rate of and the cross-section of the channel. Nie et al. showed that tuning of the diameter of the jet can be used to set the diameters of the droplets and, by appropriate adjustment of the diameters of each jet, to set the number of the inner droplets.

Similar observations were reported simultaneously by Utada et al., which used an axi-symmetric system for formation of multiple emulsions. This system was also capable of formation of double droplets, providing detailed control over the inner and outer radii. These authors reported two modes of breakup of the composite stream: dripping and jetting. In the dripping regime the compound stream broke in the orifice, while the jetting regime, the composite thread extended deep downstream into the outlet capillary. While the dripping regime produced monodisperse droplets, the jetting regime effectively prohibited fine control of the distribution of diameters of the drops. Again, the simple analysis based in the Rayleigh-Plateau instability of a liquid column allowed a correct estimate of the speed of flow at which the system crossed over from the dripping to the jetting regime, and the dimensions of the double emulsions. The cross-over between the regimes can be understood through a

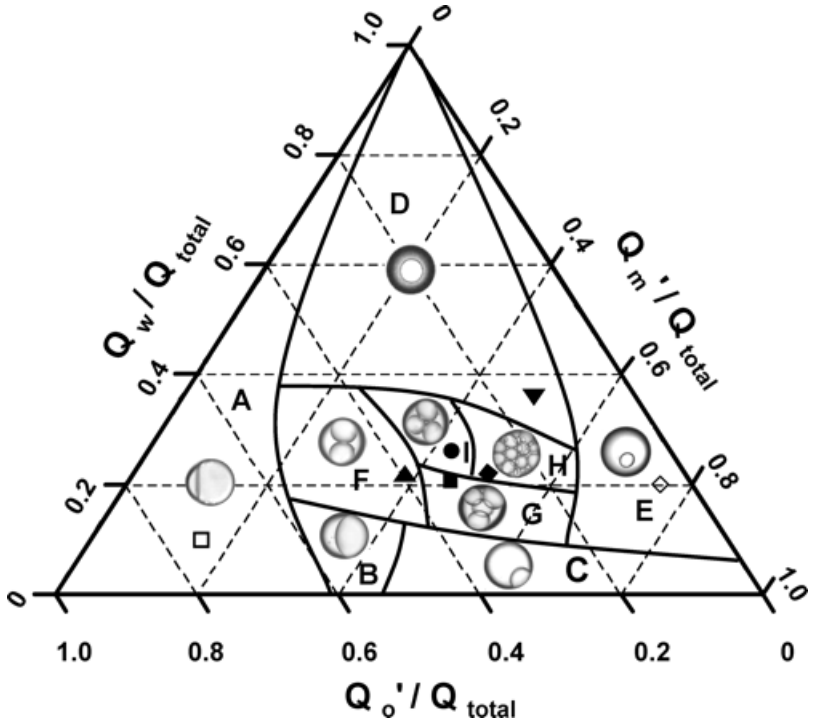

Figure 3.7: A ternary diagram that shows the structure of the double emulsions as a function of the rates of flow of the three phases (of the inner phase (Q_o), the intermediate phase (Q_m), and the outer continuous phase (Q_w).[25] Reprinted with permission from American Chemical Society.

comparison of the time needed for the perturbation of the width of the jet to grow and break-off a droplet (pinch time) with the time (convection time) needed for the compound stream to elongate into a morphology unstable with respect to Rayleigh-Plateau instability. If the pinch time is greater that the convection time, then the thread grows before it is broken off and the system crosses-over to the jetting regime. while the total rate of flow controls the breakup mode, the ratio of the rates of flow controls the volume fraction of the inner phase and the sheeting liquid, allowing fine tuning of the thickness of the shell.

In summary, microfluidic devices can be designed and constructed to successfully form multiple droplets. The stoichiometry of the droplets can be effectively controlled. It is known that flow can modify the Rayleigh-Plateau instability criteria of a column of fluid. The instability can be dived into absolute ones, which are localized in space with respect to

the walls of the device, and convective ones, which can be washed away from the orifice by the flow of either of the immiscible fluids. The subject of stability of jets of liquid subjected to both flow and confinement are an active area of study. For example, Guillot and coworkers derived the equations that predict the transition between dripping and laminar co-flow of concentrically flowing immiscible liquids in the confinement of a circular capillary. Utada et al. pointed out that this transition can be controlled by the viscous effects in the outer fluid and inertial ones in the inner liquid. As the subject is relatively new and complex, there are no practical guidelines available to date.

Rotem and others studied the formation of emulsions in a non-planar microfluidic device.[26] They found out that in a planar device, when the continuous phase wetted the wall, emulsions were formed even at the minimum flowrates of the continuous phase. In contrast, when the dispersed phase wetted the wall, the device did not produce any drops even at the maximum possible flow rate of the continuous phase. Thus, in planar devices, drop formation is strongly dependent on the wetting conditions and is only feasible in the favourable case when the continuous phase wets the walls of the microfluidic device. In contrast, non-planar devices remove the constraints on the wettability imposed by the planar geometry; drops can be formed even in unfavourable wetting conditions. With the dispersed phase flowed into a junction through an inlet, which was centered vertically with respected to the outlet nozzle, the interface between the fluids forms a spherical cap, not contacting the top or the bottom of the channel. Thus, with a fast enough continuous jet, the 3D structured device can generate emulsions with unfavourable wetting conditions. The critical conditions with the capillary number and the dynamic contact angle is showed in Figure 3.8. As the contact angle is larger than 90°, the drops are formed just like in planar devices. When the contact angle gets smaller than 90°, the capillary number, which is proportional to velocity of the continuous phase, needs to be higher to generate emulsions. With the non-planar microfluidic device, emulsions could be formed without tuning the wettability of the device.

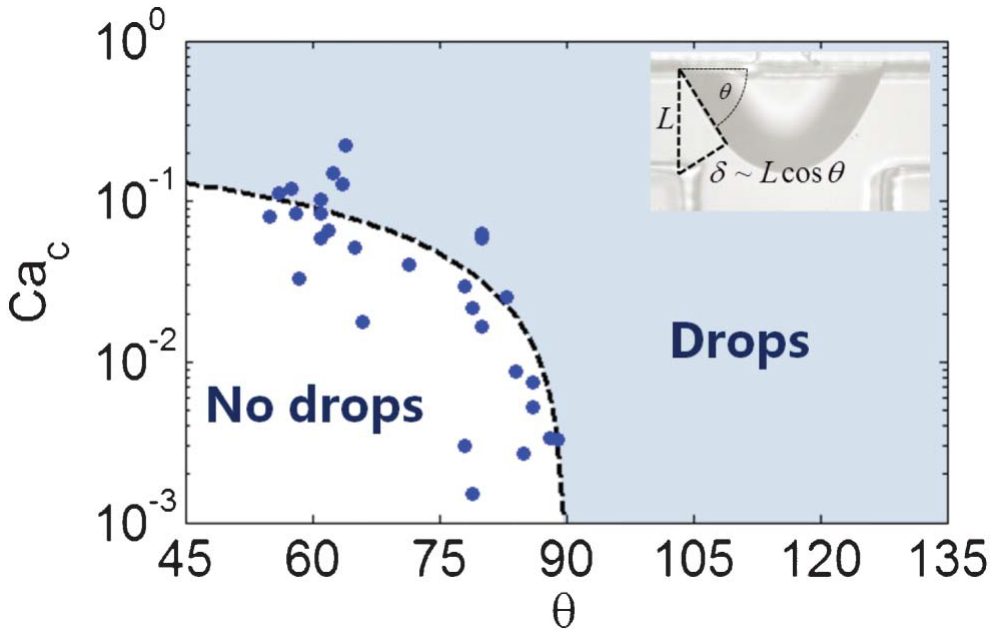

Figure 3.8: The critical capillary number as a function of the dynamic contact angle as measured for drop makers with varying geometry.[26] For θ < 90°, drops are formed only when the capillary number is higher than the critical value Ca_c. For θ > 90°, the continuous phase preferentially wets the walls and drops are formed regardless of the capillary number. Dashed line is a fit of the Cosine function to the data. Inset: approximating the cross-sectional gap δ between the side channel and the forming drop. Reprinted with permission from Royal Society of Chemistry.

Tran et al. developed a coaxial flow focusing geometry that can be fabricated using soft lithography in Polydimethylsiloxane (PDMS).[27] With a 3D channel layout, they formed a W/O/W emulsion without tuning the wettability of the channel surface. At the first junction, for the W/O emulsion, there is no need to change the wettability since PDMS favours oil. But at the second junction where the O/W emulsions are fabricated, they changed the channel height from 50 µm to 320 µm, forming an orifice in all directions. The abrupt expansion of the channels and high velocity of the outer aqueous fluid lifted the oil from the channel walls. This created a double jet consisting of the inner jet of aqueous fluid sheathed in a thin shell of oil, surrounded by the second aqueous phase. The double jet was then focused through a much narrower channel. The constriction caused the velocity of the continuous phase to increase, generating high shears that rip droplets from the end of the jet. Because

droplets were formed in the jetting regime, the droplet size were smaller than the orifice. They reached down to 14 μm in diameter for double emulsions in their device.

3.8 Gas-cored Double Emulsion in Microfluidics

Gas-core double emulsion is a less focused branch of double emulsions. Because of its viscosity and density differences to liquids, gas is usually not involved in microfluidics. However, gas can be a cheap place holder for some cases, and G/L/L is mostly utilizing this advantange.

Torza and Mason studied that in a three-phase emulsion, based on the positivity of spreading coefficients of three phases, three different equilibrium configurations can occur: total engulfing, partial engulfing, and no engulfing.[28] When the spreading coefficient of one dispersed phase is positive, the fluid would spread onto the other dispersed phase, forming complete engulfing. When all the spreading coefficients are negative, the two dispersed phases would form partial engulfing, an isotropic form. Both dispersed phases would have contact with the continuous phase. When the spreading coefficient of continuous phase is larger than zero, then the dispersed phases would not coalesce to form a single droplet. Stability diagram representing the possible morphologies is shown in Figure 3.9.

The oily bubbles we required work the best in configuration of complete engulfing. When the oily bubbles rise, because of the density difference, the oil phase would be at the bottom of the bubble. The bubbles mostly collide with particles at their tops, if the oily bubble is anisotropic, the contact interface would still be gas phase, which has weaker interaction than the oil phase. Thus, tuning the interfacial tensions, thus spreading coefficient is essential to the generation of oily bubbles.

Wan and others introduced gas-cored double emulsion in 2008.[30] They fabricated PDMS microfluidic devices with flow-focusing and T-junction design to generated gas-in-water-in-oil (G/W/O) emulsion. Multi-core droplets were also generated with the aid of surfactant

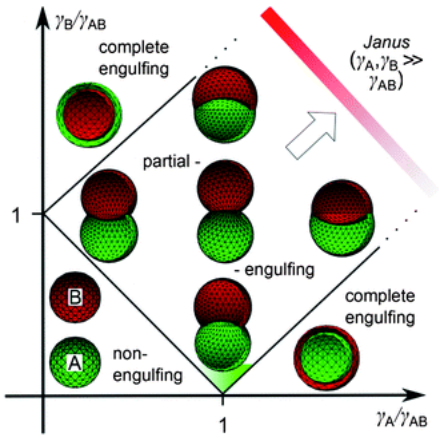

Figure 3.9: Stability diagram representing the possible morphologies of a double droplet of phases A and B. γ_A is the surface tension of phase A, γ_B is the the surface tension of phase B, and γ_{AB} is the interfacial tension between phase A and B.[29] Reprinted with permission from Royal Society of Chemistry.

presented in water phase. Acrylamide and photoinitiators were added into the water phase and the product emulsion was treated with UV light for the polymerization of water phase. The emulsion polymerized and formed porous microparticles and the pores were created because of the bubbles entrapped. The final product is shown in Figure 3.10.

The strongest drawback of using microfluidics for the generation of oily bubbles is the low production rate. Since the channel sizes are in um, the flowrates are usually below 1 mL/min, to accommodate the laminar flow required for generating emulsions. However, in a lot of the cases, this is not enough. There are currently several attempts to generate double emulsions in parallel.

Jeong et al. presented 400 parallelized channels of generation of uniform gas bubbles in 2017.[31] they fabricated a 3D PDMS microfluidic devices with ladder geometry while the junction of emulsion generation is planar. Since the single emulsion with flow focusing devices was well established before, they focused more on the coefficient of variation (CV) between different channels. By controlling the pressure between a small range (0.138 mPa and 0.179 mPa), the CV can be dropped to less than 5% of around 50 µm bubbles. They

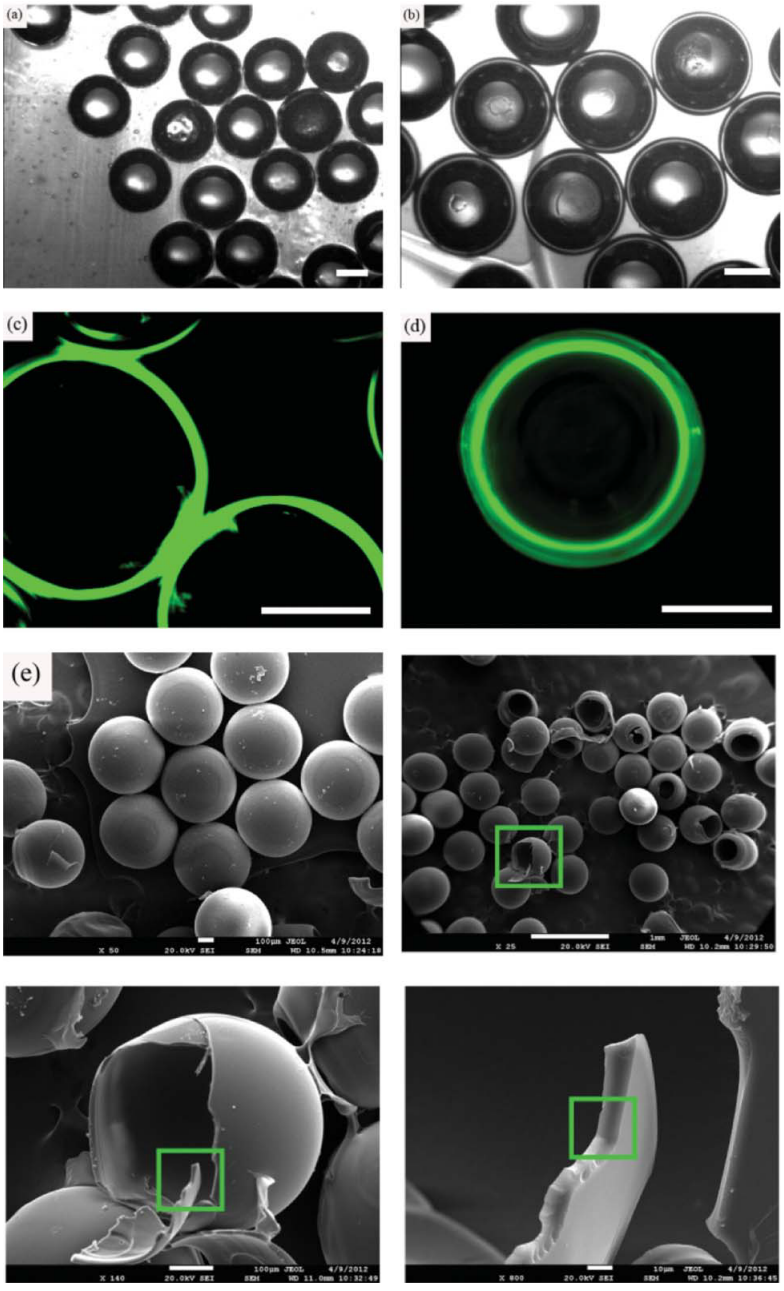

Figure 3.10: The microscope, Laser scanning confocal microscopy (LSCM) and Scanning electron microscopy (SEM) photograph of the hollow microspheres after polymerization. (a) and (b) Microscope photograph hollow microspheres with different shell thickness. (c) and (d) LSCM photograph of hollow microspheres with different shell thickness. The scale bar is 300 mm. (e) SEM image of 1,6-hexanediol diacrylate (HDDA) hollow particles.[30] Reprinted with permission from Royal Society of Chemistry.

suggested also the polydispersity was mostly caused by the fabrication error. Overall, they produced monodispersed microbubbles at 1L/h in 400-channel devices.

Later they fabricated another 400-parallelized-channels microfluidic device to generate gas-cored double emulsion.[32] With 3D structured flow-focusing channels, even PDMS channels can generate hydrocarbon oil as dispersed phase. They generated both G/W/O and G/O/W emulsions. With the CV of less than 5%, they generated 10^{11} compound bubbles in less than an hour. They presented a rare earth element (REE) extraction within the microfluidic device by adding ions inside the water phase. After mixing with the oily bubbles, the ions in aqueous phase were completely extracted to oil phase within 10 seconds. The efficiency is much higher than the common mixer-settler scheme.

Another potential method was proposed by Eggersdorfer et al. in 2017.[33] Using tandem emulsification, they injected the single emulsions fabricated in the first device into the second one to achieve double emulsion. They use a step-emulsification device because of its expansibility and robustness, but the same method can also be used for flow-focusing device. They generated W/O/W emulsions at a rate of 20 mL/h with 200 nozzles, which is around 80 droplets per second per nozzle. However, this method has a major drawback when generating oily bubbles. Because of the absence of surfactant in oil phase, the bubbles generated at the first devices would coalesce before they enter the second one.

4 Research Methodologies

The overall setup is shown in Figure 4.1. A glass microfluidic device is fabricated in cleanroom and mounted on a microscope. With the three phases injected into the device in proper order and proper flowrates, the oily bubbles form at the outlet section of the device.

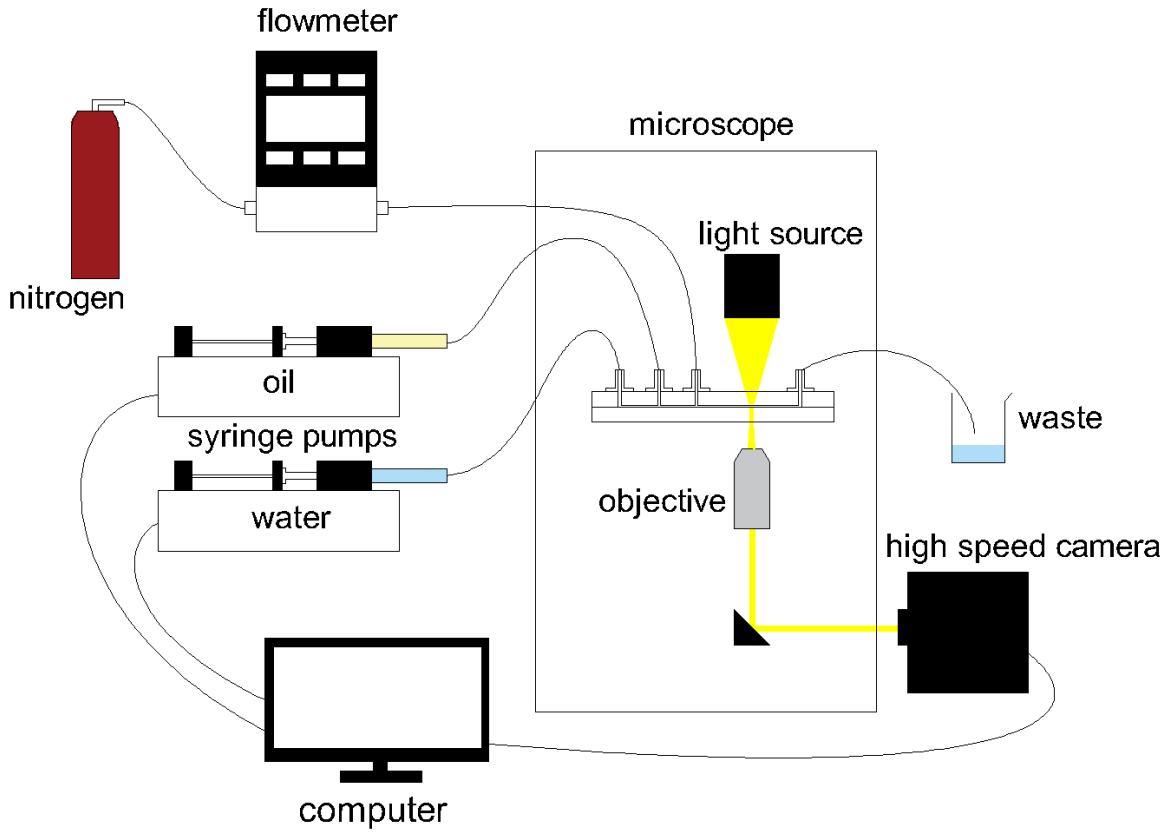

Figure 4.1: Schematic of the experimental setup.

4.1 Fabrication of Polydimethylsiloxane (PDMS) Microfluidic Devices

Pattern Design

The pattern is designed using KLayout, a free integrated device layout editor.

Photomask Fabrication

The design was then written on the photomask, which consist of chrome on soda-lime glass,

by laser lithography.

Substrate Cleaning

The silicon substrate was immersed in a piranha solution to remove any dust before any other processes.

Coating of photoresist

The mold used for PDMS device that we fabricate is SU-8 2050 (Microchem), a high contrast, epoxy based negative photoresist designed for micromachining and other microelectronic applications. We spin-coated a layer of negative photoresist onto the substrate. The photoresist requires soft-baking on a hot-plate.

Pattern Forming on the Photoresist

The substrate was placed on a mask aligner and covered by the patterned photomask. The substrate was then flooded with UV light. The transparent part on the photomask would result the aligned photoresist to react and be cross-linked while the opaque part would result the aligned photoresist not to react and still be soluble. The substrate was then immersed in the developer (SU-8 Developer). After this step the pattern would be shown on the substrate.

Fabrication of PDMS devices

A mixture of PDMS and curing agent was poured onto the mold and baked in an oven. The PDMS was then peeled off from the mold and bonded with glass slides or other PDMS under weigh.

4.2 Fabrication of Glass Microfluidic Devices

Pattern Design

The pattern is designed using KLayout, a free integrated device layout editor.

Photomask Fabrication

The design was then written on the photomask, which consist of chrome on soda-lime glass, by laser lithography.

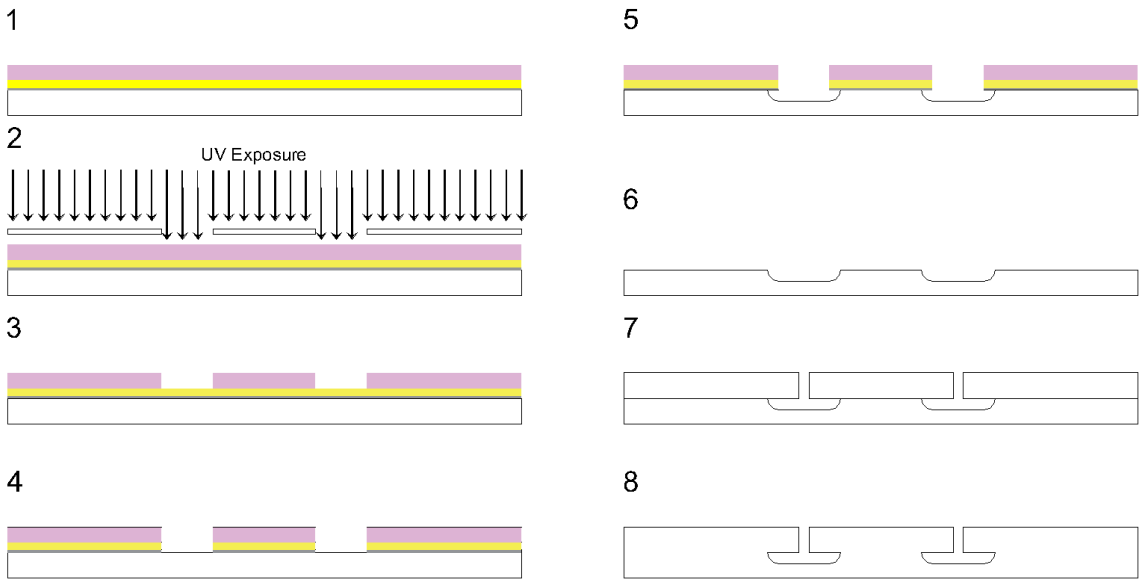

Figure 4.2: Steps for the fabrication of glass microfluidic devices. Pink represents photoresist, yellow represents gold, white represents glass.

Substrate Cleaning

The glass substrate was immersed in a piranha solution to remove any dust before any other processes.

Sputtering of Chrome and Gold Layer

A layer of chrome and a layer of gold was sputtering onto the substrate, works as a protection layer for HF etching.

Coating of Photoresist

A photoresist is a light-sensitive material, occurring chemical reaction which change its physical properties. The positive photoresist would be soluble to the photoresist developer after exposing to UV light, while the unexposed portion remains insoluble. We spin-coated a layer of positive photoresist (HPR504) onto the gold layer of the substrate. Step one in Figure 4.2 is the result after this step.

Pattern Forming on the Photoresist

The substrate was placed on a mask aligner and covered by the patterned photomask. The substrate was then flooded with UV light. The transparent part on the photomask would result the aligned photoresist to react and be dissolved while the opaque part would result the aligned photoresist not to react and insoluble. The substrate was then immersed in the developer (Microposit 354 developer). After this step the pattern would be shown on the substrate. Step three in Figure 4.2 is the result after this step.

Metal Etching

The remaining photoresist in the last step works as a protection layer for metal etching. The substrate was immersed in gold etchant and chrome etchant to remove the metal where the photoresist does not exist. This would write the pattern onto the metal layers. Step four in Figure 4.2 is the result after this step.

Glass Etching

The remaining metal layers in the last step works as a protection layer for HF etching. The substrate was immersed in borofloat etchant. The height of the channel was controlled by etching time. Because of the nature of homogeneous etching, the cross-section of the channel would be in shape as shown in Figure 4.3. Step five in Figure 4.2 is the result after this step.

Figure 4.3: Cross-section of the channel

Removal of Remaining Photoresist and Metal Residue

the remaining photoresist was removed by acetone and isopropanol. The metal residue was removed by their respective etchant. After this step, the preparation of patterned substrate finished. Step six in Figure 4.2 is the result after this step.

Port Drilling

Holes were drilled on a blank substrate of the same material to be inlet and outlet ports. The substrate would be holed substrate.

Glass Bonding

Both patterned and holed substrates would be cleaned with piranha solution followed by soap. Then the substrate would be aligned and pressed together. The substrate would be bonded, and the etched glass part would become sealed channel. Step seven in Figure 4.2 is the result after this step. If we would like the device to endure higher pressure, we could anneal the glass, to make the bonding permanent. Putting the glass device into the Muffle furnace and heating it at 600 °C for two hours would result in Picture eight in Figure 4.2.

4.3 Materials

N-dodecane (>98%, Fisher Scientific), oleic acid (technical grade, Fisher Scientific) were used as received. Fluorite (Boreal Science) particles were prepared by crushing and grinding with jaw crusher and grinding machine, respectively. After sieving with 400 mesh sieves, the particle batch has a D_{50} of 14 μm.

4.4 Liquid Handling

Four streams were injected into the device: gas phase (dispersed phase), oil phase (middle phase), water phase (continuous phase), and slurry. The gas phase is nitrogen (99.998% purity), the oil phase is dodecane with different concentration of oleic acid, the water phase is milli-Q water with different pH tuned with the slurry, and the slurry is different concentration of mineral microparticles dispersed in water. The flowrate of gas phase (Q_G) is controlled by gas flowmeter (Fishersci), the flowrate of oil phase (Q_O) and water phase (Q_W) is controlled by syringe pumps (Cole Parmer compact syringe pump) and syringes (Hamilton 5 mL syringes).

4.5 Setup for Microflotation Test

Because of fittings between the tubing and the device, there are reservoirs where the oily bubbles can collide. The sudden flowrate drop may cause a lot of coalescence. Further down at the tubing, because the flow is upwards at first, the oily bubbles flow faster than the surrounding water phase, and can accumulate at the top of the tubing, causing coalescence as well. In conclusion, we did not manage to extract the oily bubbles outside of the chip using tubing and fitting.

Thus, we replace the outlet port into a mL-sized column. The column was prepared by drilled a hole at the end of a 4.5 mL cuvette and glue it upside down on the microfluidic chip as shown in Figure 4.4. A pipette is used to transfer the slurry or the ionic solution into the column. Because the microfluidic chip also injecting liquid, we only add 2 mL of solution into the column. For mineral flotation, another high-speed camera is placed on the side of the column to observe the oily bubble rising from the chip. To study oily bubble-mineral interaction, another method was also tested. We inject the slurry into the channel as another inlet channel, which will mix with the stream containing oily bubbles.

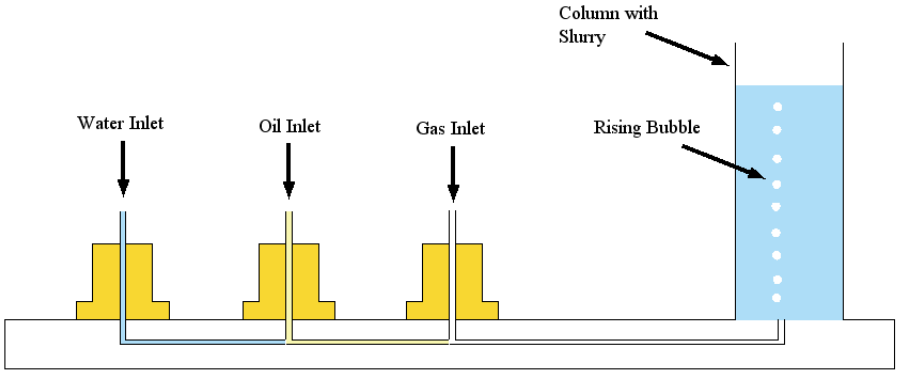

Figure 4.4: Schematic of microflotation on a microfluidic device

4.6 Observations

The mix streams were observed on a microscope (Zeiss Axiovert 200M) and the images were mostly captured by high speed camera (Photron FASTCAM MINI AX 100) at 1000 frames per seconds and a shutter speed of 10 µs. The magnification of the objective is 10 times. The images were later analyzed with MATLAB and ImageJ.

4.7 Work Flow of Processing Image Sequences

Since our gas flowmeter does not present the flowrate of gas correctly, we need to use the microscope to calculate the gas flowrate by counting overall volume of the gas flow through within a certain time. The volume of the bubbles are calculated by counting the pixels within a microscope image such as shown in Figure 4.5.

Step 1. Change the image to greyscale and deduct it from the average picture. This step can remove any dust shown in the image. The result image would be like in Figure 4.5 B.

Step 2. Threshold the greyscale images to two sets of black and white images, one with both gas-oil and oil-water interfaces, the other with just G/O interface. As shown in Figure 4.5 B, the brightness of interfaces are different. with right threshold, in this case, 65/255 and 184/255, would give an image with both interfaces, Figure 4.5 D, and only gas-oil interface, Figure 4.5 C. This way, we can calculate the area just for the air bubble and the area for overall oily bubble. This step is done in ImageJ.

Step 3. The output of last step is in a series tiff file, we run a small MATLAB program change them back to a series of png files.

Step 4. With a MATLAB program, we can determine where is the bubble. However, we record the images in 1000 frames per second, a bubble in the first image would also appear in the second image. Thus, we tell the program which bubble is the same one in different images, and it will calculate the velocity of this bubble by dividing the movement by the

Table 4.1: Interfacial tensions between phases used in the generation of oily bubbles

Outer Phase	Inner Phase	Interfacial tension (mN/m)
Water	Air	72.8
Water	Dodecane	51
Water	0.5% Oleic Acid in Dodecane	31
Dodecane	Air	25
0.5% Oleic Acid in Dodecane	Air	25

given time. Since our stream is quite stable within the one second record time, all the bubbles travels at a similar rate.

Step 5. A MATLAB program can now calculate how many distinct bubbles/droplets travel through in front of our camera within a given time. The area for the gas and oil for our examples is shown in Figure 4.5 E.

Step 6. With all the given information, we can calculate the gas flowrate, oil flowrate, gas bubble sizes, oily bubble sizes and other information.

4.8 Interfacial Tension Measurement

The interfacial tensions between different phases were measured by optical tensiometer (Biolin Scientific Theta Lite). The syringe contains inner phase and the environment is outer phase. In our three-phase system, the density of the phases increases from inside to outside, therefore, the inner phases are always lighter than the outer phases. Thus, a reversed needle is required to form a reversed pendant drop. With the setup as shown in Figure 4.6, the inner phase is pushed out of the syringe and forms a pendant drop. The curvature of the drop is affected by the surface tension and gravitational force. By analysing the radii change with respect to height, it is possible to determine the surface tension in this method. By the built-in function of the software, we determine the interfacial tensions within our systems as in Table 4.1.

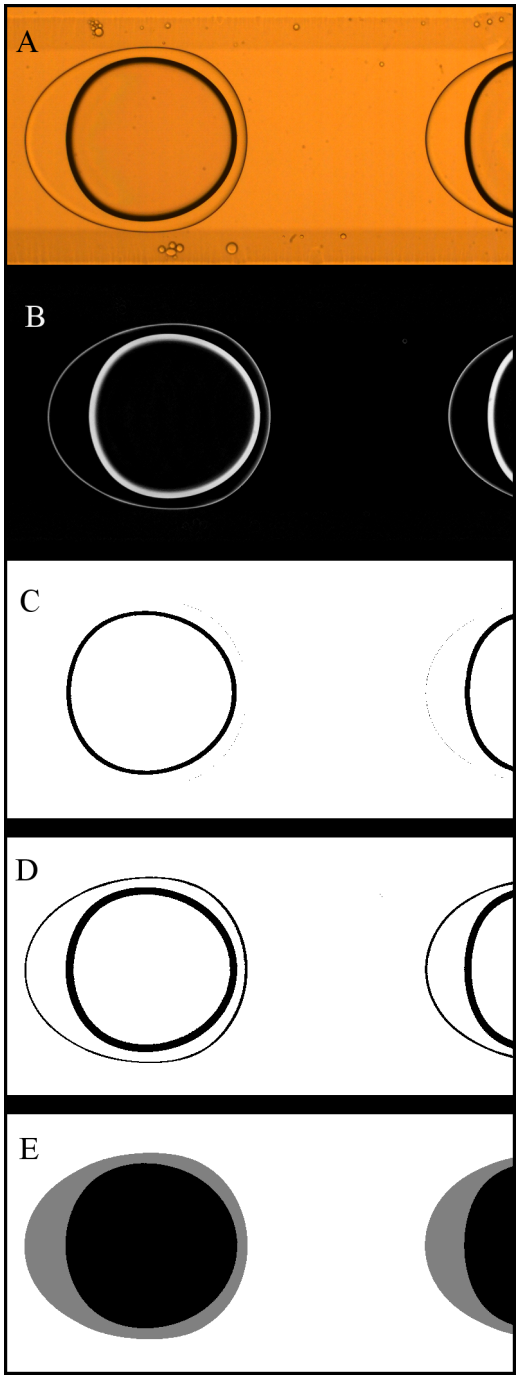

Figure 4.5: (A) Original caputred image of an oily bubble. (B) Greyscale of (A). (C) Black and white image showing oily bubbles. (D) Black and white image showing just bubbles. (E) A schematic presenting how much of the area we count for the air and gas. The black represents gas and the grey represents oil.

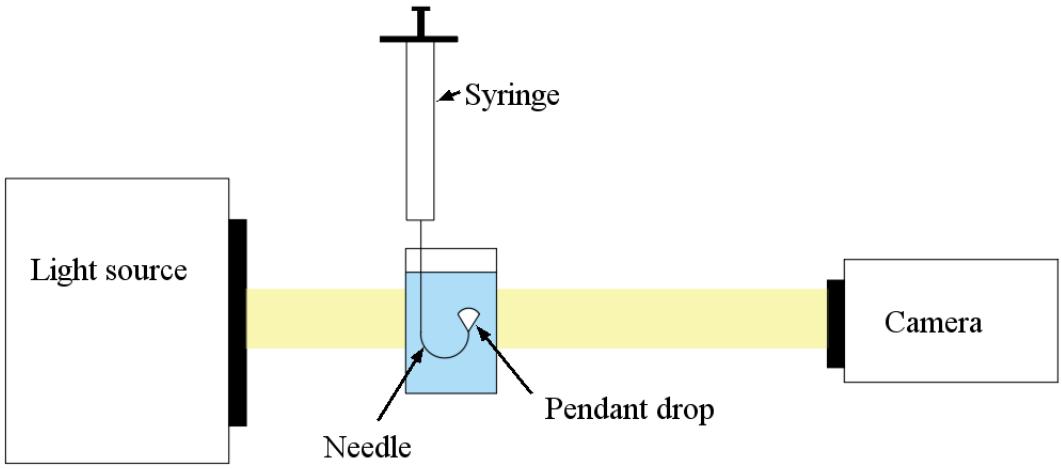

Figure 4.6: Schematic of interfacial tension measurement with a reverse pendent drop

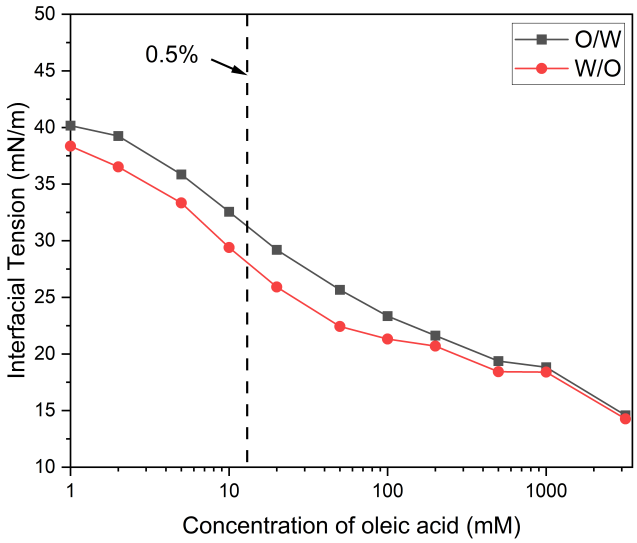

Figure 4.7: Interfacial tension between dodecane and water against concentration of oleic acid in dodecane. O/W indicates oil drop in water measurements. W/O indicates water drop in oil measurements.

As shown in Figure 4.7, the interfacial tension between dodecane and water decreases as concentration of oleic acid in dodecane increases. The differences between the two lines in the figure is because the collector is in oil phase. When the oil phase is continuous phase, the collector is more abundant, thus lower the interfacial tension. In our case of reactive oily bubble, the oil is middle phase, which is dispersed compared to water, thus the O/W curve is more accurate. As we stated before, as the spreading coefficient is positive, total engulfing is achieved. The collector, oleic acid favors oil-water interface than oil-gas interface. Hence, we can assume the gas-oil interfacial tension is constant along the concentration of collector. Because of its low Hydrophilic-lipophilic balance (HLB) value at 1, at low concentration of oleic acid, they do not enter the water phase. Hence, the water-gas interfacial tension remains the same. Therefore, in our case, the concentration of oleic acid tunes the spreading coefficient. According to the calculation, very tiny amount of oleic acid can change the spreading coefficient to positive. However, in microfluidic generation of emulsion, the contacting time and formation of droplets is within milliseconds, the collector does not have enough time to occupy all the interface, thus higher concentration of collector is required. The concentration of the oleic acid should be too high as well. As the proportion of the oleic acid become significant, some of the collector go into the water phase, reducing the water-gas interfacial tension. This may result the spreading coefficient to negative.

5 Design of Microfluidic Devices

5.1 Design of PDMS Devices

We firstly tried the fabrication of microfluidic devices with PDMS because its ease to fabricate. The first generation of design is shown in Figure 5.1 of a planar design (same depth everywhere). For design A, the intersections are more compact to give room to the outlet zigzag section. While for design B, there is a longer channel between the two intersections and the outlet section is much shorter. However, as Rotem showed in their study,[26] no emulsions can form with the material favours dispersed phase (oil phase). We did not generate double emulsions in these devices.

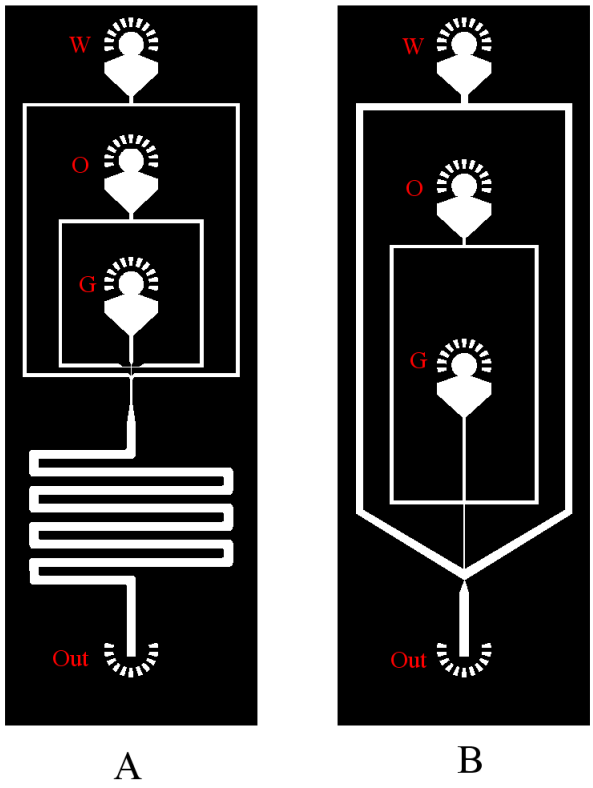

Figure 5.1: Design for planar PDMS microfluidic devices. W represents water inlet, O represents oil inlet, G represents gas inlet, and Out represents outlet port. The smaller rectangular shapes around the inlet and outlet ports are markers for visual port punching.

We also tried to fabricate a 3D-structured microfluidic device by adding another layer of photoresist. The water phase section and the outlet section were changed to deeper channel as shown in Figure 5.2. Instead of bonding PDMS onto a glass slide, we bonded two PDMS slabs together. As shown in Figure 5.2, A1 and A2 is a pair and B1 and B2 is another pair. We deepen the channel for the water phase because PDMS favours oil instead of water. If the emulsion (oil droplet/oily bubbles) do not contact the channel wall, it is still possible to ignore the hydrophobicity of the device material and generate emulsions. However, with only one kind of photoresist we have, we are unable to create a channel with a ratio between orifice height and overall height small enough. The size of emulsions increases with the size of the orifice. Because of the low viscosity and density of gas compared to liquid, the bubbles generated are always going to be big enough to touch the side of the channel. Examples are shown in Figure 5.3, as the outlet stream is a co-flow of bubbles in water with oil.

5.2 Design of Glass Devices

5.2.1 Device for the Generation of Reactive Oily Bubbles

We firstly used the design in Figure 5.1 to fabricate a glass microfluidic device, however, because of the difference between how the tubing connects to the channel, it did not work. For PDMS devices, we only need to punch a 1.75 mm hole in one of the slabs and push the tubing into it. Because of its thickness and elasticity, PDMS can hold the tubing. However, glass device does not have these properties. Therefore, a connection is required to hold the tubing. The connections are too big to fit on a 22 mm by 8 mm device planned for PDMS. Therefore, we need a new design, a more spacious one, for the glass microfluidic device.

We started with design A in Figure 5.4 since we would like to see the oily bubbles evolve in longer time inside the device. However, with the outlet length too long and too narrow, the pressure drop formed at this section is too high. The requirement for the gas pressure

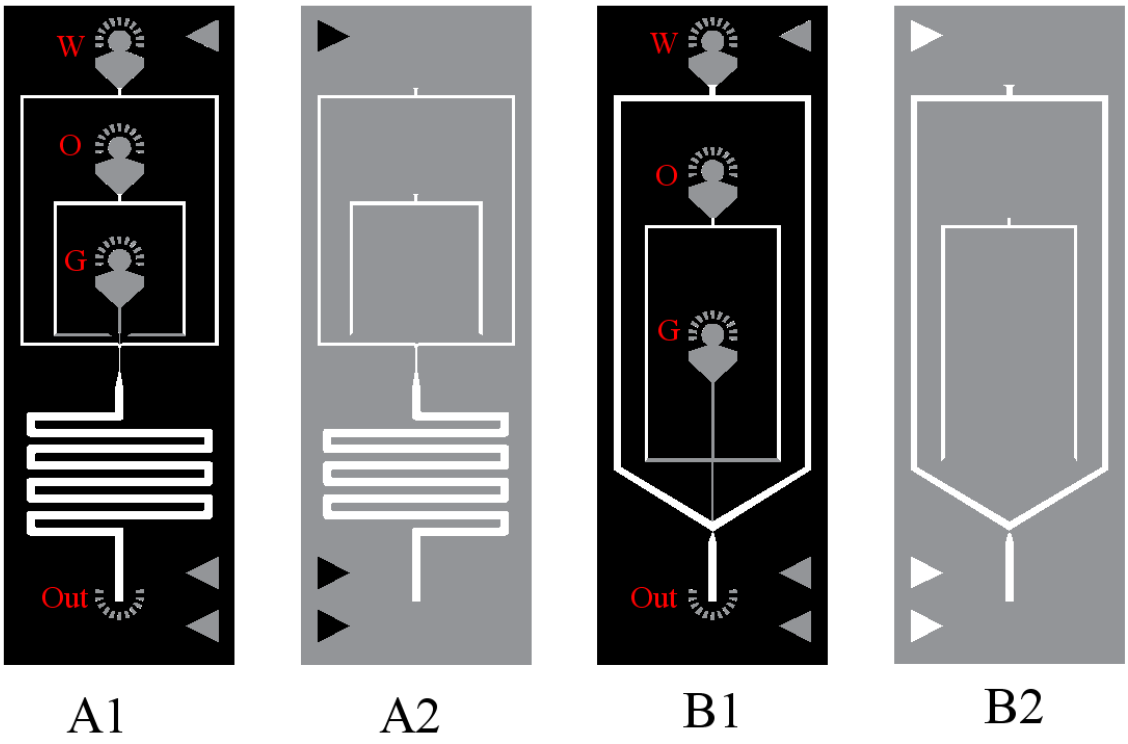

Figure 5.2: Design for 3D PDMS microfluidic devices A and B. White represents a depth of 100 µm (two layer of photoresist), grey represents a depth of 50 µm (one layer of photoresist), and black represents a depth of 0 µm (no photoresist). W represents water inlet, O represents oil inlet, G represents gas inlet, and Out represents outlet port. The smaller rectangular shapes around the inlet and outlet ports are markers for visual port punching. The triangles on the sides are for channel alignment. Since the grey triangles on side 1 are receding and the black triangles are protruding, when we are trying to align them, they fit each other.

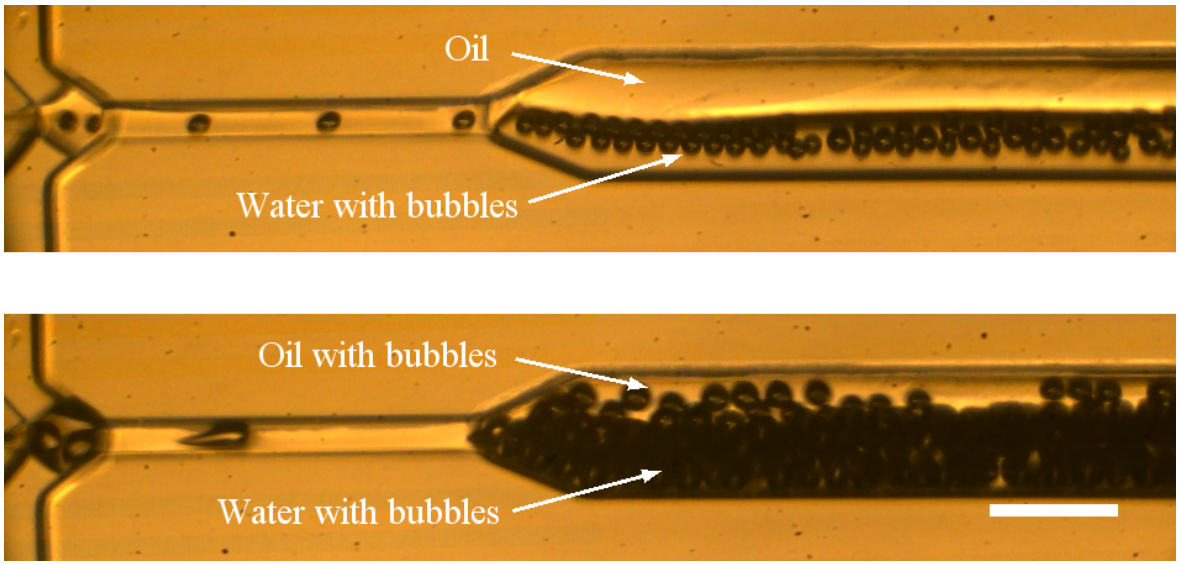

Figure 5.3: Microscopic images of generation of co-flow of bubbles in water with oil. Scale bar is 200 µm.

inlet quickly rose up to 40 psig which is too high for the temporary glass bonding. We tried annealing the glass device for a higher tolerance of pressure. However, because the threshold to the outlet is too high, the inlet stream easily flows back to other inlet streams. We tried to create a new outlet port after the second turn at the zigzag section. The oily bubbles can form now, however, we are unable to observe this because the size of the nanoport is too big that it covered the viewing area at the generation.

We soon changed the design to Figure 5.4 B. We successfully generate oily bubbles in this design. We tried to guide the oily bubbles out of the microfluidic device by using the nanoport, they coalesced at the end of channel. Because of fittings between the tubing and the chip, there are reservoirs where the oily bubbles can collide with each other. The sudden flowrate drop caused a lot of coalescence. Further down at the tubing, because the flow was upwards at first, the oily bubbles flowed faster than the surrounding water phase, and accumulated at the top of the tubing, causing coalescence as well. In conclusion, we did not manage to extract the oily bubbles outside of the device within a tube. We tried with thinner outlet channel shown in Figure 5.4 C, the coalescence occured as well. We found

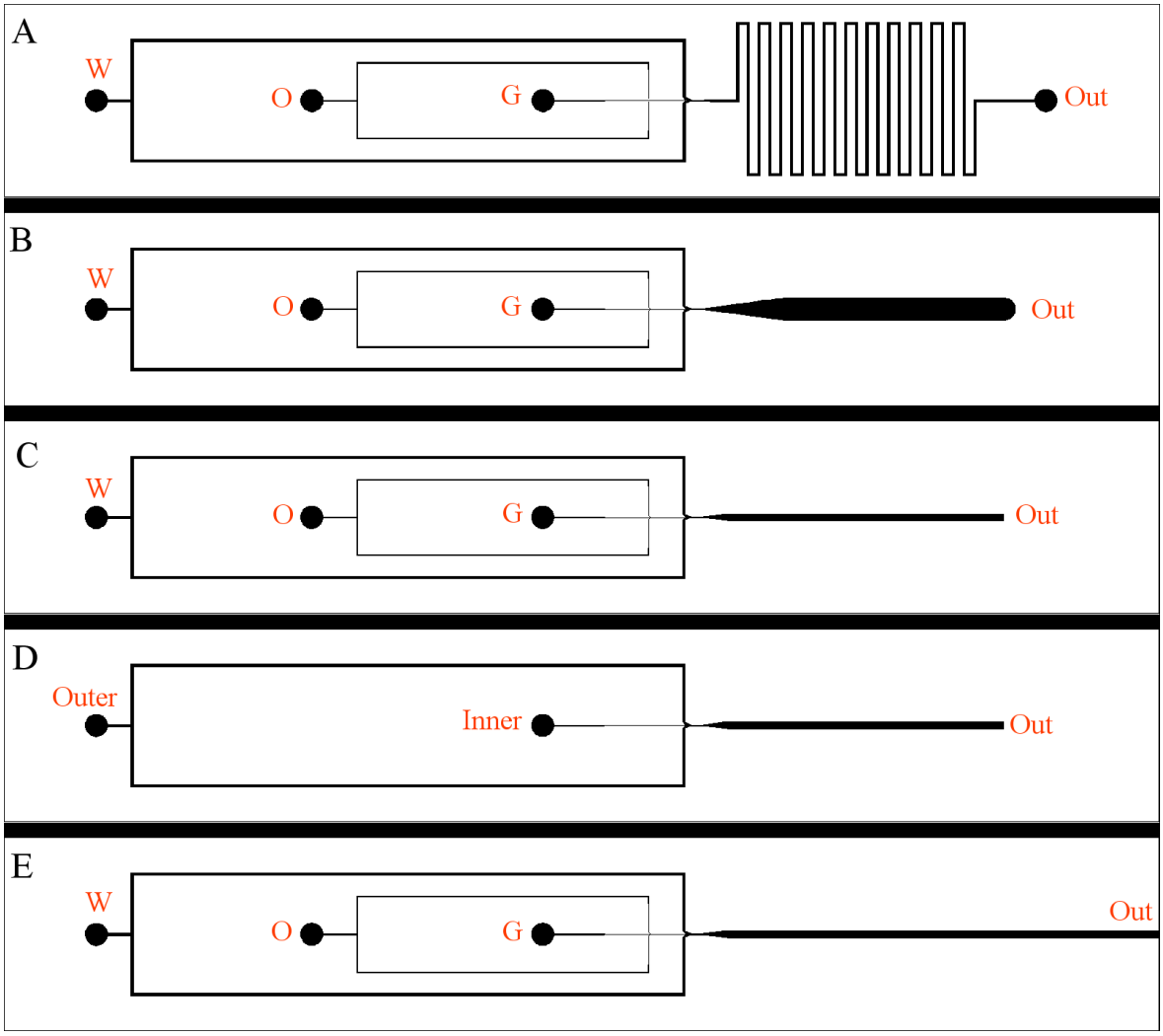

Figure 5.4: Diagram of each genereation of microfluidic design for the generation of oily bubbles. W represents water inlet, O represents oil inlet, G represents gas inlet, Out represents outlet port. in (D), Outer represents inlet port for outer phase (continuous phase) and Inner represents inlet ports for inner phase (dispersed phase).

out that the design within the channel is not the problem, therefore, we finalized with design C. In comparison with design B, the thinner outlet channel offers a faster velocity where the oily bubbles do not collide each other inside the channel. We also tried two modifications on the general application of the device. With the design D in Figure 5.4, we removed one of the inlet ports, thus we can generate single emulsion. This was used for the generation of reactive oil droplets or air bubbles which is at similar size with reactive oily bubbles for further comparisons. With design C, we can achieve similar function by closing one of the nanoport. However, the section with no flow still affected the flow. Because the nitrogen gas has some compressibility, the empty channel worked as a big reservoir and the pressure drop after each generation of bubble was higher. The air bubbles generated in design C would be larger and fewer than in design D at the same gas and water flowrates.

We also extended the outlet channel further to the end of the device. Instead of drilling a hole for the outlet stream to exit the microfluidic device, the oily bubbles can discharge from the side of the channel. Thus, we can submerge the entire device under water in a much bigger tank and have the oily bubbles flown from the side of the device. In this way we can attach these oily bubbles onto upside of a hydrophobic material and do some other experiments like Atomic Force Microscope. We also tried to drill an outlet hole at a similar position as the other designs. The hole drilled was much larger than the microfluidic channel, resulting most of the outlet stream including all the oily bubbles went through the drill holes, while some of the water phase continued flowing through the microfluidic channels. In this way, part of the water generated could be recycled, and the addition of the water to the flotation column could be less problematic. This idea could evolve into a two-way outlet port, with one concentrated with oily bubbles and the other containing only water. The efficiency of the system improves and the amount of the material decreases.

We also tried tuning the dimensions of the channel near the intersections to study how they affect the generations of oily bubbles. Figure 5.5 A shows a detailed version of the

intersections within our device. As for Figure 5.5 B, we changed the inlet width for water phase to 40 μm. The water flowrate can be much lower because the cross-section area is smaller. However, with less water in the outlet stream, the void fraction (gas percentage) increases, and the bubbles colliding with each other. With the absence of surfactant in the continuous phase (water phase), the emulsions are more likely to coalescence. The design could be improved by decreasing the outlet stream width, thus the bubbles would be less likely to collide. However, in this way, it would be similar to design A, if the channel depth could be shallower. In contrast, a shallower design A requires less oil and water, and generated more and smaller oily bubbles.

We also tried to decrease the channel width of the gas inlet for an easier stream of co-flow of gas and oil phases after the first intersection. As we showed in the next chapter, a co-flowing stream is the most desired situation for our generation of reactive oily bubbles.

5.2.2 Device for the Mixing of Reactive Oily Bubbles and Mineral Particles

About studying the interaction between reactive oily bubbles and mineral particles inside the microfluidic device, we had four designs. Firstly we tried with our design in Figure 5.6 C, replacing the water phase to the slurry. Jeong et al. presented the same method with the rare earth element removal from the water phase.[32] However, as the particles are different from the ions, they do not flow similarly as the ions. With this method, most of the particles would be either attached to the oily bubbles upon formation or not colliding at all within the device. Therefore, we introduced a method where there is a mixing stage within the device. With Figure 5.6 A, we split the outlet stream into two channels and combine them with the slurry inlet and mix them with a straight line. With Figure 5.6 B, it is a similar idea with design A, we add a further section of zigzag mixing stages to improve the collision efficiency. We also added four more outlets trying to study the effect of amount of mixing involved on the flotation efficiency. With Figure 5.6 D, which is the most likely to our previous design

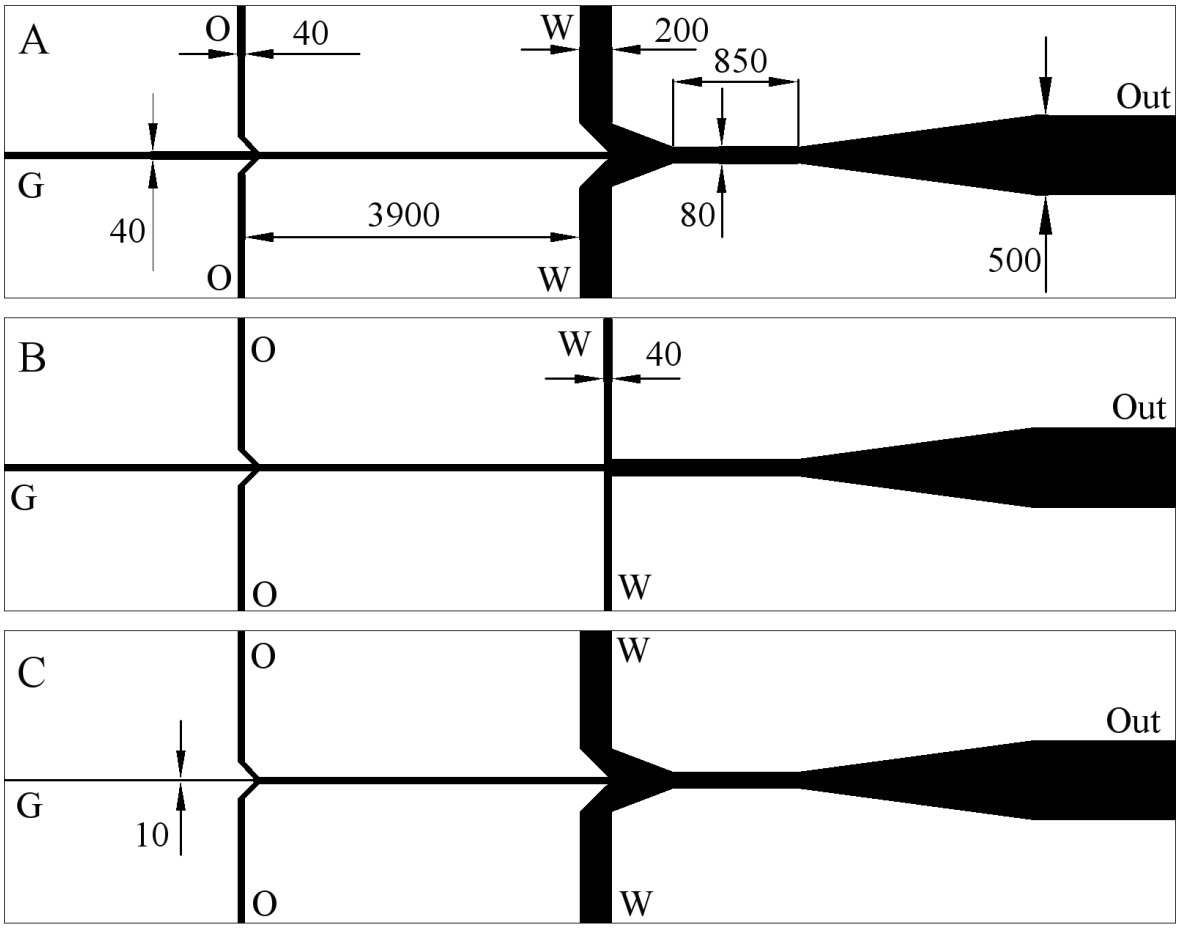

Figure 5.5: An enlarger version of both intersections within our devices (A) and its slight modification (B and C). B and C only shows where it has difference from A. Numbers are in unit of μm.

for the generation only, add a side channel introducing the slurry. With Figure 5.6 C, where generation design and mixing design both changed, we can study how large amount of reactive oily bubbles interact with particles. Design C and D both presented same problem, where the bubbles do not collide with particles much. Because the slurry stream was introduced on one side, it is very likely for the stream to co-flow in the outlet stream and never collides. This can be improved if there is an induced mixing stage or much longer straight outlet channel. In design B, the oily bubbles colliding each other in the zigzag mixing section, and the particles were stuck in the corner where the oily bubbles never reach. With design A, because there are two sharp turns after the oily bubbles were formed and a split junction, the morphology of reactive oily bubbles is not the same at the mixing stage compared with when they were just generated.

Of our choices for the channel depth, 20, 30, 40, 50 μm, the particles with a D_{90} of 35 μm are very likely not to pass through the channel and block the channel. We also improved our design by etching the port-drilled plate with 100 μm for the particles to flow freely. The cross section of the channel becomes to Figure 5.7. The results would be shown in the next chapter.

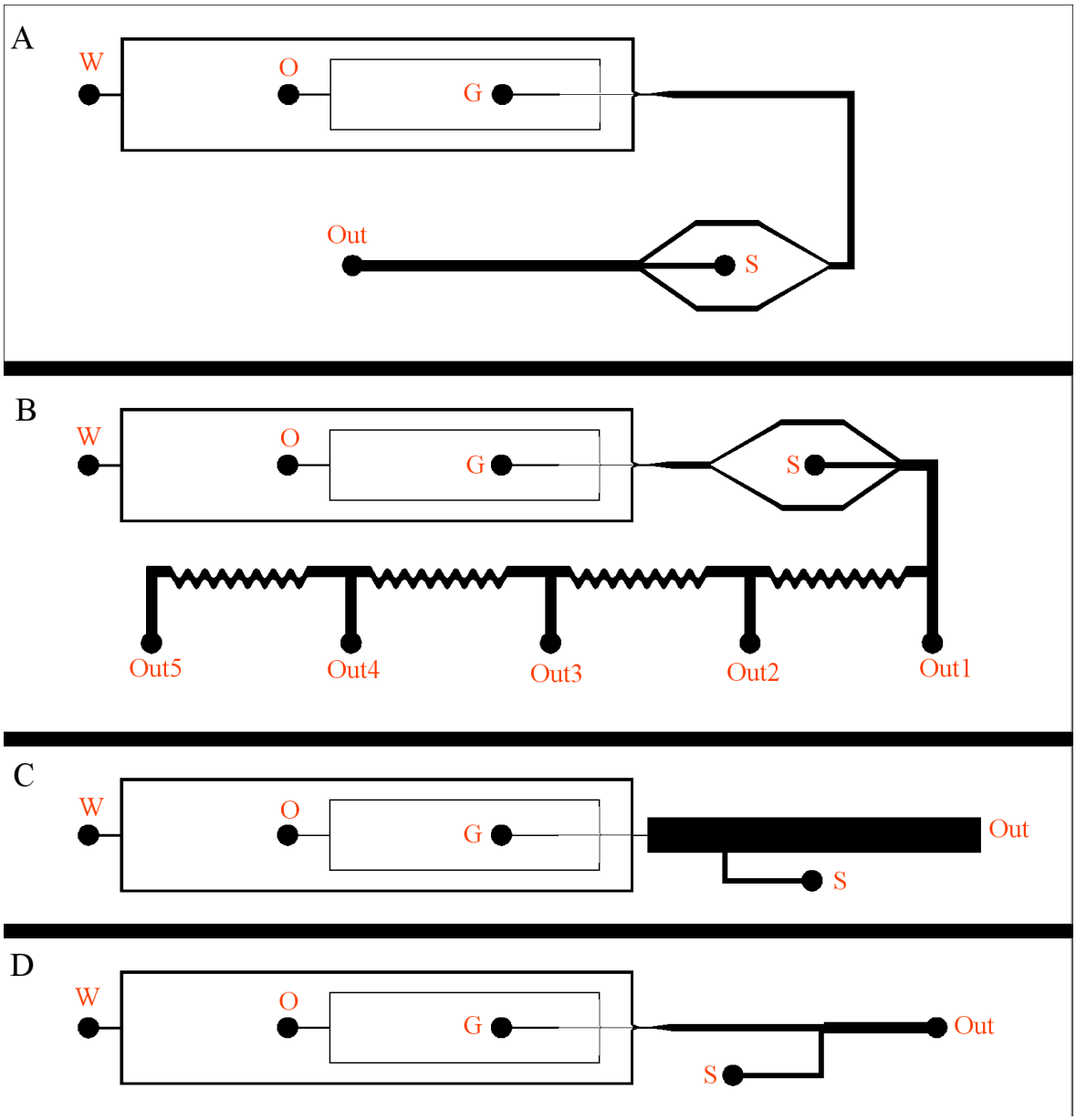

Figure 5.6: Diagram of each genereation of microfluidic design for generation of oily bubbles and mixing of oily bubbles and slurry. W represents water inlet, O represents oil inlet, G represents gas inlet, S represents slurry inlet. Out represents outlet port.

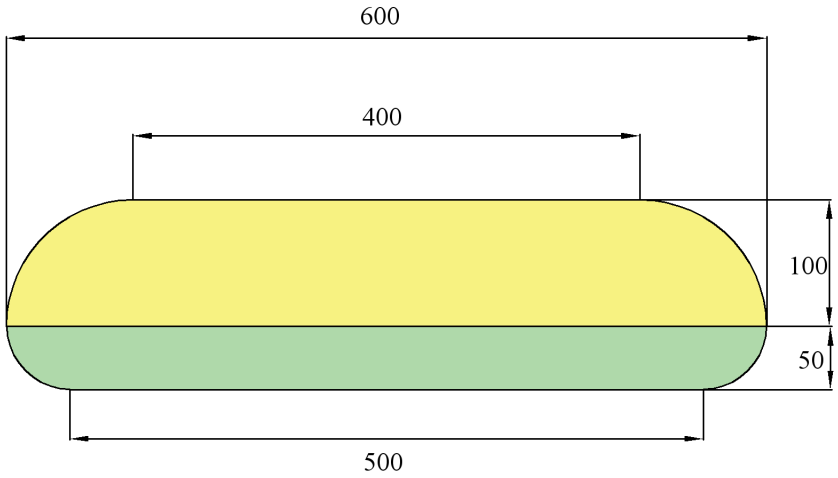

Figure 5.7: Cross-section of a channel with both glass substrates etched. In order to match a channel with width of 500 µm in the photomask and depth of 50 µm, shown in light green, the other half should be design to have a width of 400 µm and a depth of 100 µm, shown in light yellow. The final channel would have a maximum of width of 600 µm, and a maximum of depth of 150 µm. All number is in µm.

6 Generation of Reactive Oily Bubbles and their Applications

6.1 Generation of Reactive Oily Bubbles

6.1.1 Flow pattern

We conducted experiments of generating emulsions inside of a 50-μm-height-channelled microchip. With the tuning of different flowrates of water, oil and gas, different flow patterns can be formed. Mostly they can be categorized into 5 sections. They are oily bubbles only, oily bubbles with bubbles (Zone V), oily bubbles with droplets (Zone II), oily bubbles with droplets and bubbles (Zone IV), and no emulsions formed. The oily bubbles only are separated into two different zones: normal oily bubbles (Zone III) and thin-layered oily bubbles (Zone VI), since these two zones have different mechanism of generation of oily bubbles. The no emulsions formed section can also be separated into two zones, co-flow of bubbles in oil and water (Zone I) and co-flow of gas, oil and water (Zone VII). All these zones can be found on with flowrates in Figure 6.1 and their appearance in Figure 6.2.

Zone VI and Zone VII are separated from the others by a straight line where the flowrate ratio between gas and oil is high enough, no bubbles formed at the first intersection inside the chip. When the flowrate of water is high enough to generate bubbles, they are in Zone VI forming thin-layered oily bubbles. And on the other case, flowrate of water is not high enough, they co-flowed to the outlet. We do not have any data points in Zone VII, because we do not have a method to determine the flowrate of gas without them forming bubbles.

Zone I is separated from Zone II, III, IV, V by a straight line where the flowrate of oil is high enough, that the bubbles are formed in oil while stream of water failed to break the oil stream. It results as a co-flow stream of bubbles in oil and water.

Among Zone II, III, IV, V, they are separated from each other by two crossing lines. The

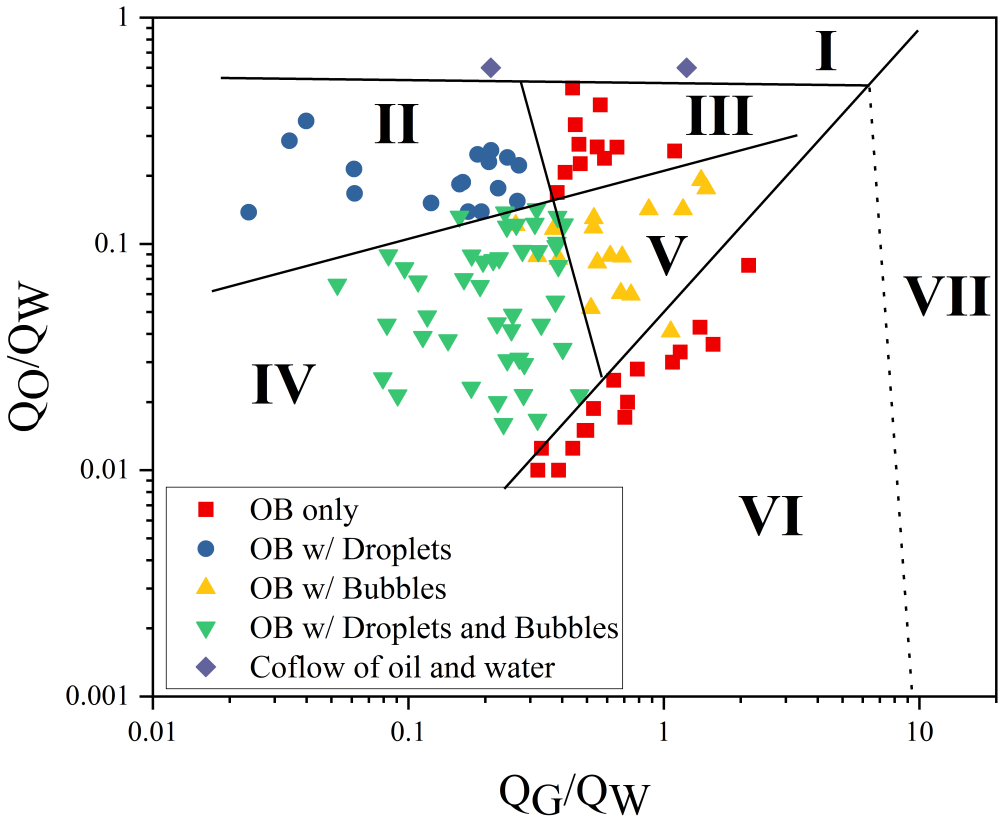

Figure 6.1: Different flow pattern at different flowrate ratios between gas and water phases (Q_G/Q_W) and between oil and water phases (Q_O/Q_W)

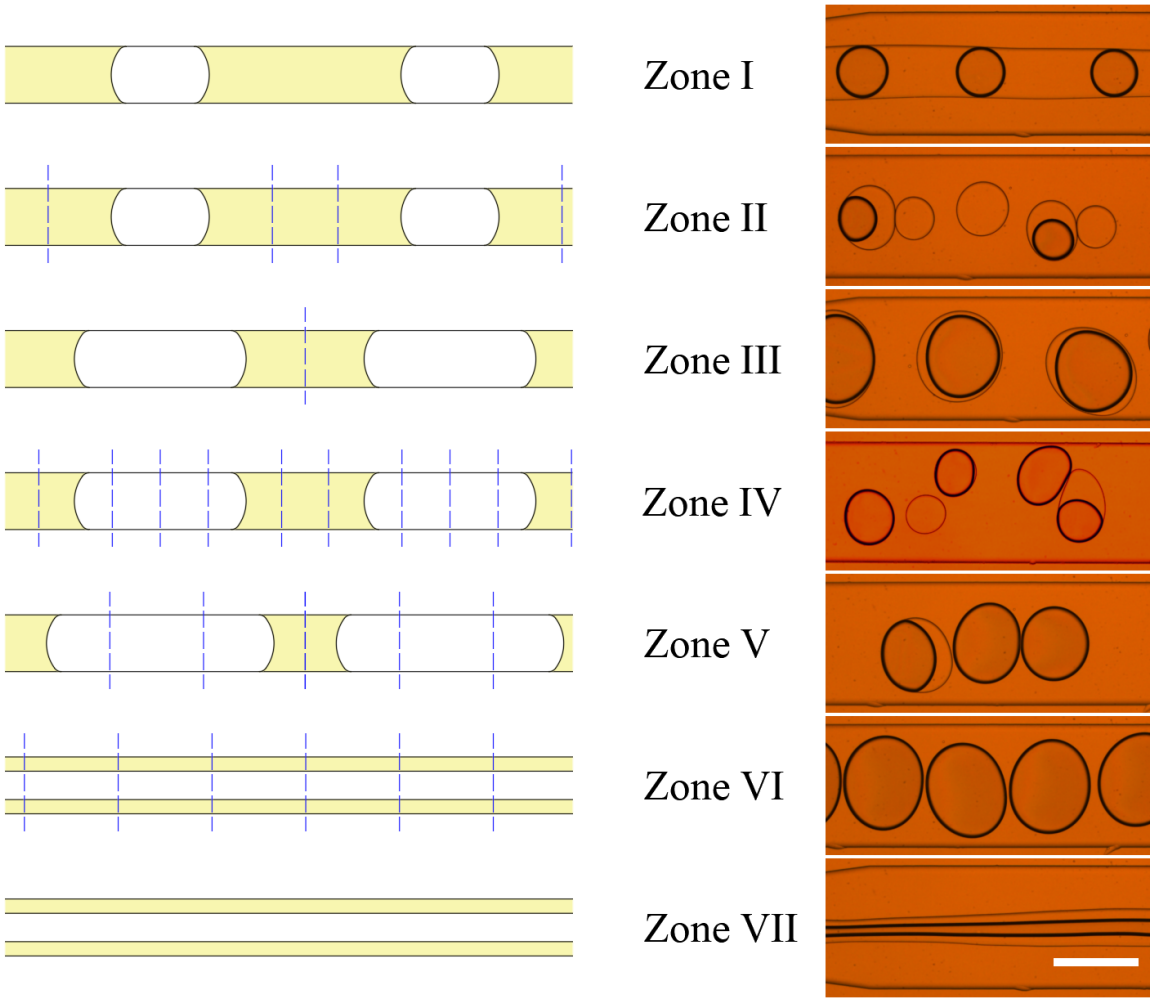

Figure 6.2: A schematic and actual microscope images of different zones. Left panel indicate the situation after the first intersection and where the water would cut the stream. Yellow represents oil phase, white represents gas phase and blue lines represent where the water would cut the stream and form emulsions. In Zone I and Zone VII, the water flowrate is too low to cut any stream, therefore, no blue lines present. Right are the corresponding actual formation in the channel after the second intersection. The darker borders are gas/liquid interfaces and thin borders are oil/water interfaces. Scale bar is 400 μm.

positive gradient line separating whether the outlet stream has bubbles or not (between Zone II, III and Zone IV, V) and the negative gradient line separating whether the outlet stream has droplets or not (between Zone III, V and Zone II, IV). In all these regions, bubbles are formed at the first intersection, and double emulsions are formed at the outlet stream. From the point of view in Zone III, where only oily bubbles formed, you must decrease only the flowrate of gas instead of increasing the flowrate of oil to have some droplets inside the outlet stream. On the other hand, you have to decrease only the flowrate of oil instead of increasing the flowrate of gas to have some bubbles.

6.1.2 Oily Bubble Size

In our case of study, we found out that thin-layered oily bubbles (Zone VI) suits our interest the most. With the gas phase occupies most of the volume inside the emulsion, the specific surface area of oil is maximized. The amount of oil and collectors can be minimized in the process. Because of the high gas/oil flowrate ratio required as shown in Figure 6.1, the oil flowrate is neglected to determine the size of oily bubbles. The relation between the size of thin-layered oily bubbles and the gas/water flowrate ratio under different height of channels is shown in Figure 6.3 A. As it is clearly shown, when the channel is higher, the bubbles are bigger. When the flowrate ratio is below 1, the size of oily bubbles increases as the ratio increases. However, when the ratio is higher than 1, the size seems to reach a plateau and, in some cases, decreases.

When we divided the diameter of the bubble by the diameter of the orifice for each of the channel, we get Figure 6.3B. The dimensionless sizes of the bubble have a similar trend for 30 μm, 40 μm, and 50 μm. The disagreement of 20-μm-height channel with the others may be caused by the different aspect ratio. With the intended width of 40 μm, 20-μm-height channel results in an aspect ratio of 4, while the other three channels have the aspect ratio of 3.3, 3, 2.8, for 30 μm, 40 μm, and 50 μm, respectively.

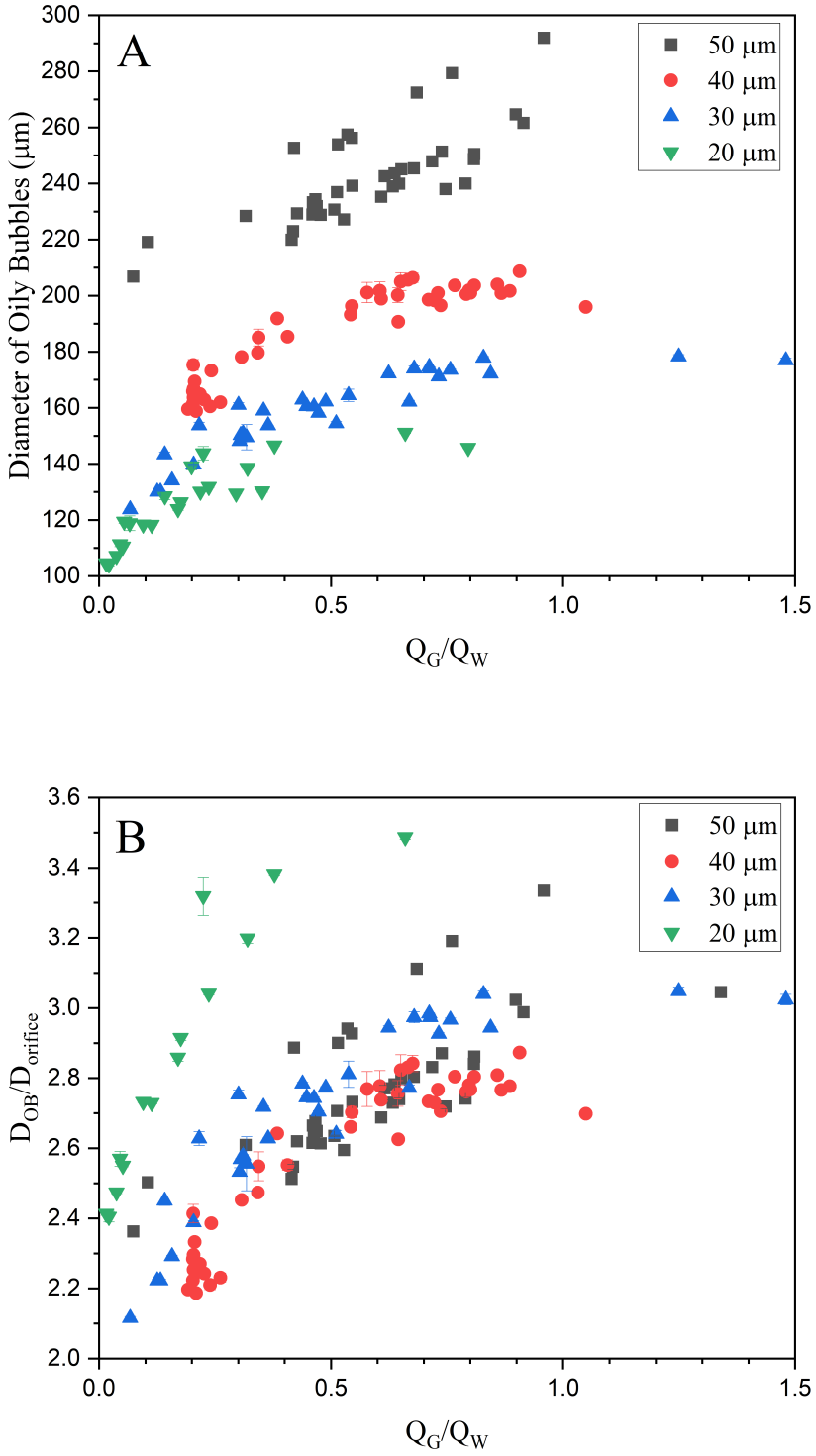

Figure 6.3: The bubble size against flowrate ratio between gas and water phases in different height of channels.

We compared the flow pattern of thin-layered oily bubbles with bubbles in water without any surfactants in the same 30 μm height channel, and it is shown in Figure 6.4. The size of the air bubbles always increases, but the size of the oily bubbles increases and reach a plateau, as also shown in Figure 6.3. Figure 6.5 shows some captured images of air bubbles and oily bubbles under low and high flowrate ratios. Under low flowrate ratios, the air bubbles and oily bubbles behave the same, small bubbles with much distance between them, and water is the dominant occupant. In contrast, under high flowrate ratios, the flow patterns are quite different. The air bubbles as shown in Figure 6.5 C are quite big in each one of them and occupy the whole channel leaving some gap of water between each of them, while the oily bubbles are in smaller form. In Figure 6.5 D, the oily bubbles flows as two rows, interleaving between them. This happens when the aspect ratio of the channel is higher. When we perform the same experiments with a 50-μm-height channel, the oily bubbles clump in the centre line, squeezing each other, and leaving the side lines clear for water. Because of the collectors in the oil layer, reactive oily bubbles do not coalesce in milliseconds, they are able to exist in such form. In our case, the oily bubbles generated would be discharge into a much larger column where the oily bubbles were separated further. If they are pumped into a more planar reservoir in the microfluidic device, they may merge into bigger oily bubbles.

6.1.3 Oil Cap

In Figure 6.6, we show a thin-layered oily bubble in generation. The last oily bubble breaks at 0 ms. The tip of the new bubble shrinks before 0.4 ms and stays similar until around 1 ms. In the meantime, the redial length of the bubble increase. After 1 ms, the bubble becomes wider and longer. At 1.8 ms, the oil caps at the front of the new bubble and at the back of departed bubbles are both visible. At 3.2 ms, the oil cap is not visible anymore. At 5.2 ms, the bubble is about to break. 0.07 ms later, the bubble break, but the oil phase is still connecting two bubbles. At 5.33 ms, the oil phase breaks, and the cycle is complete. The oil droplet visible

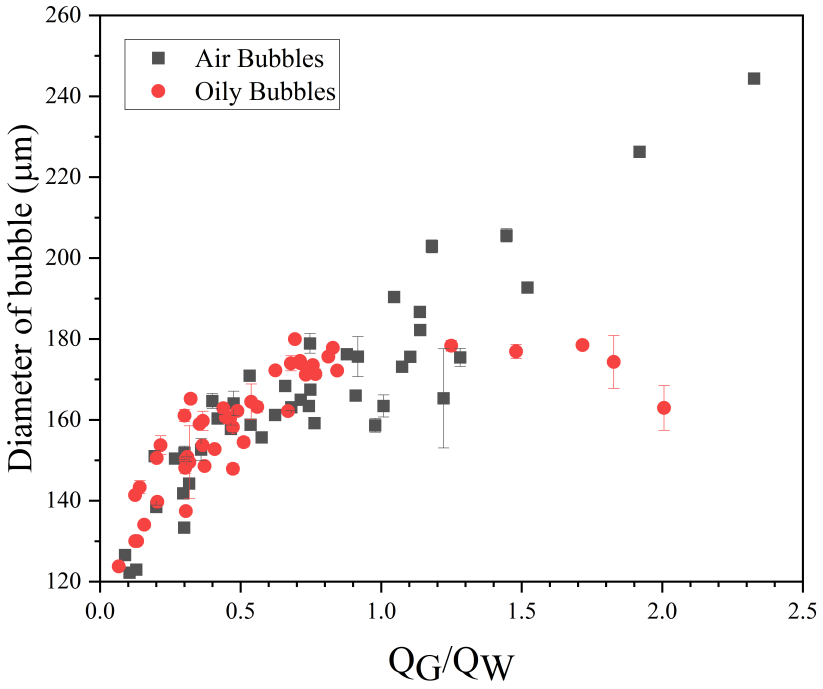

Figure 6.4: The bubble size against flowrate ratio between gas and water phases for air bubbles and reactive oily bubbles in the same channel.

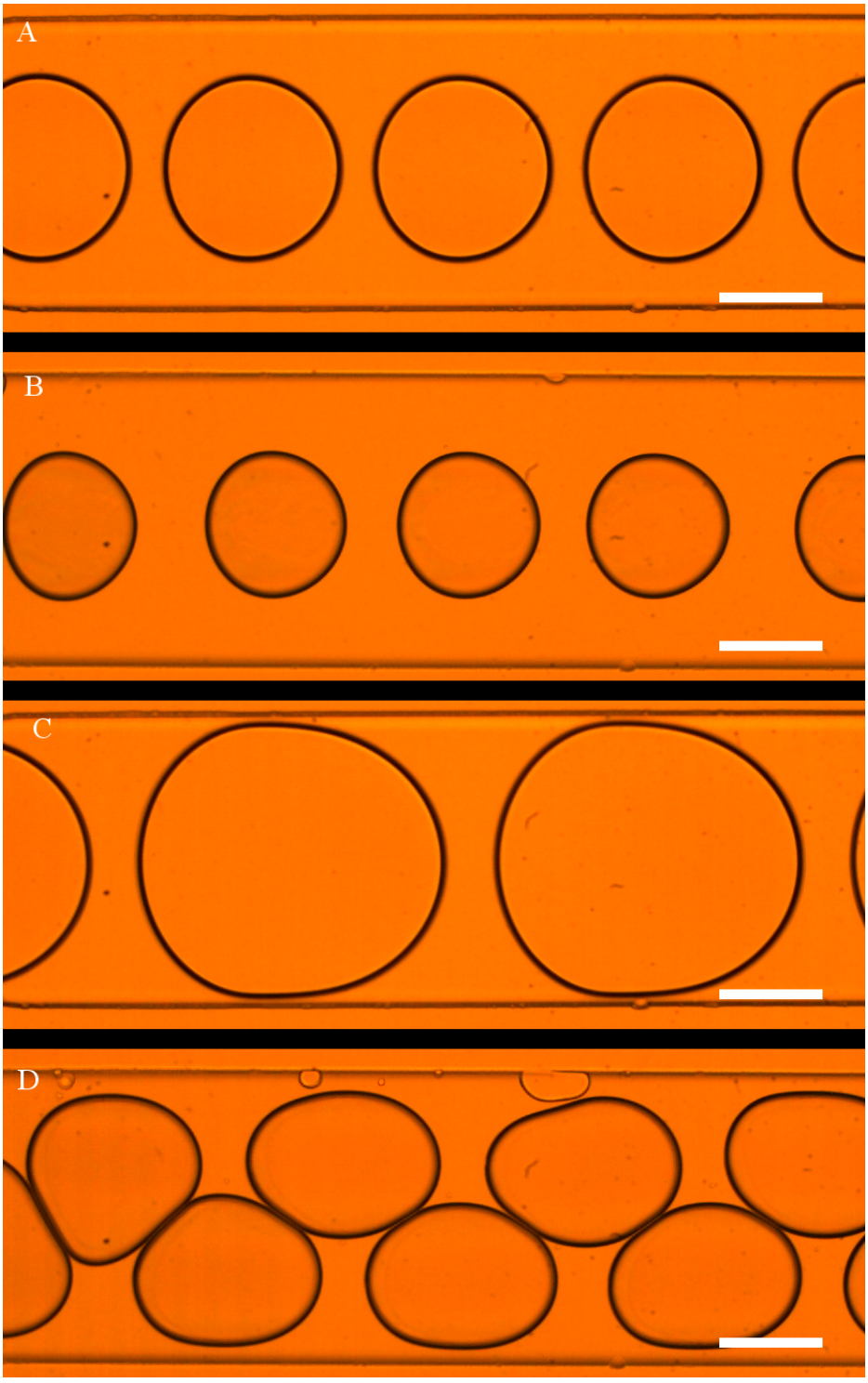

Figure 6.5: Morphology of the bubbles (A, C) and thin-layered reactive oily bubbles (B, D) under low (A, B) and high (C, D) flowrate ratio between gas and water phases. Flow direction is to the right. Scale bar is 200 μm.

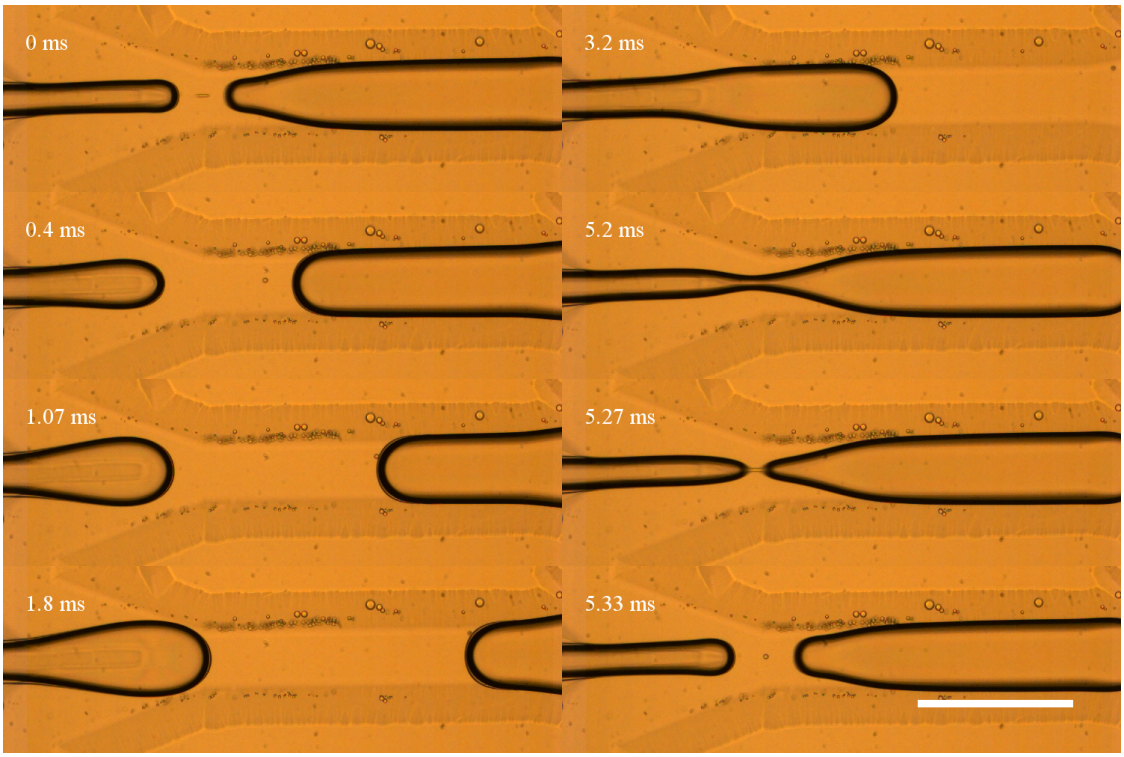

Figure 6.6: Generation of a thin-layered oily bubble. Flow direction is to the right. Scale bar is 400 μm.

at the breaking of the oily bubble is around 14 μm in diameter. According to our calculation, the oil present in the oil droplets only accounts for less than 2% of the oil input, the rest are in the oil layers of oily bubbles. As the thin-layered oily bubbles flow further into the channel, the oil cap at the end become less obvious. As shown in Figure 6.7, the oil layers are only visible just after the oily bubbles were generated because of the narrow channel. As the sphericity of the bubble goes higher through the channel, the oil cap spread around the bubble and become less visible under the microscope. As calculated by distributing oil equally to each bubble, the oil layer would be around 1 μm. As the resolution of our high speed camera is 2 μm, it is impossible to observe the oil layer with our microscope.

We also tried generating non-reactive oily bubbles with our microfluidic devices. Some examples are shown in Figure 6.8. The oil cap on the bubble shows a higher contacting angle at the bubble-water interface. Some of them, as one shown in Figure 6.8B, have two oily

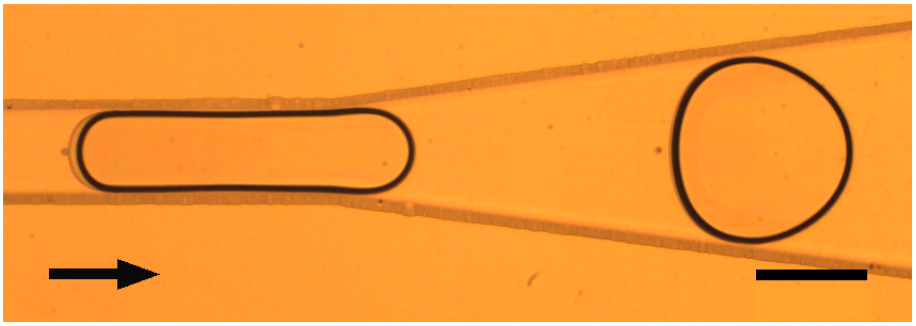

Figure 6.7: Evolution of a thin-layer reactive oily bubble inside the channel. Arrow in the bottom left corner indicates flow direction. Scale bar is 200 µm.

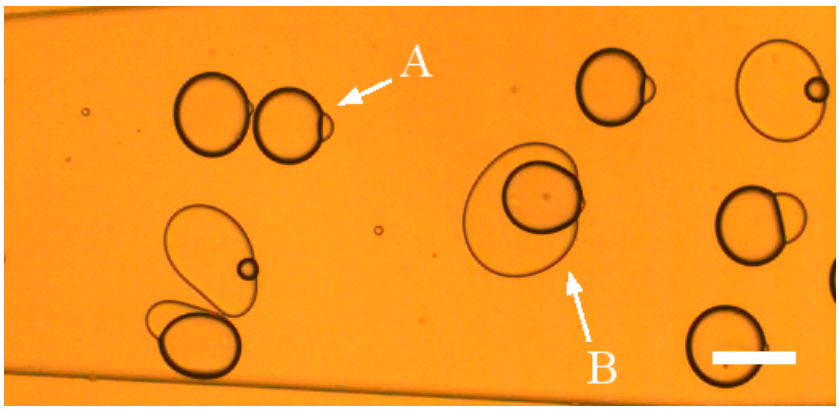

Figure 6.8: Examples of partial engulfing non-reactive oily bubbles. Flow direction is to the right. Scale bar is 100 µm.

patches on the bubble, which would not be possible if the oil phase can be move freely along the interface. As stated before, this would not be efficient, comparing to reactive oily bubble, because of their lower oil coverage.

6.2 Application of Reactive Oily Bubbles

6.2.1 Microcolumn Flotation

Microcolumn flotation were constructed as stated in subsection 4.4. As it is shown in a sequence of images in Figure 6.9, a bubble with visible oil layer at the bottom attracted some mineral particles at the bottom of the oil layer. Because of the magnification required

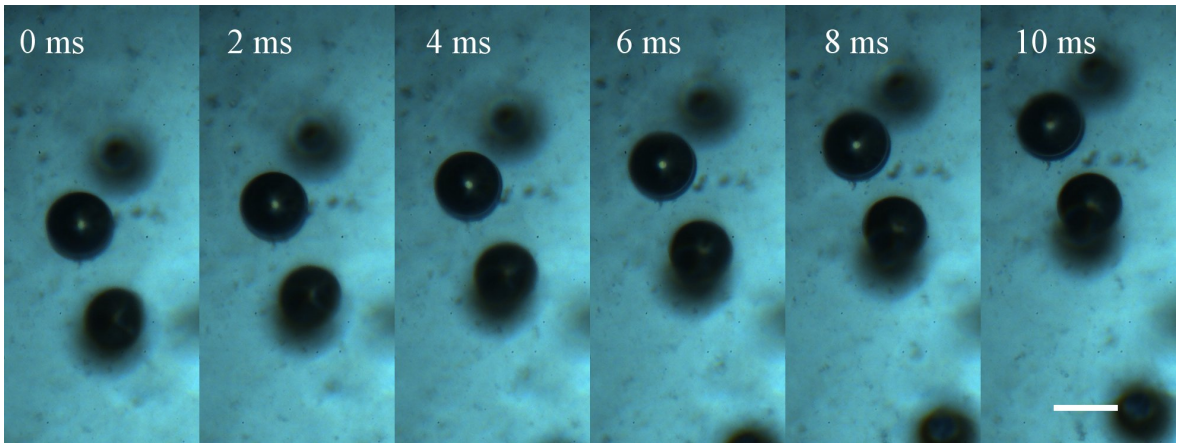

Figure 6.9: Sets of captured images showing a rising oily bubble with particles attached in focus with several rising oily bubbles out of focus. Scale bar is 200 µm.

to see the oily bubble, the depth of field is very narrow. Most of the bubbles are out of focus. It is very hard to conclude whether they have particles attached or not. With the outlet not confined by the nanoport, there is another method generating reactive oily bubbles with less water. With the flow at Zone VII, when the coflow stream reach the reservoir, the pressure suddenly drops, forcing the oil and gas stream to break up into oily bubble form. The mechanism is quite similar comparing to Zone VI, while this method is more passive and harder to control. As shown in Figure 6.1, Zone VII has higher flowrate ratio between gas and water phases, thus, Zone VII would use less water in the generation of oily bubbles. Zone I can also be broken up using the same method, however, with most of the inner phase consisting of oil, they are more likely to generate oil droplets than oily bubbles.

6.2.2 Bubble-particle Interaction within Microfluidic Device

With slurry introduced into the microfluidic channel, we can observe the interaction using a microscope. Figure 6.10 shows several examples of reactive oily bubbles loaded with fluorite particles. In Figure 6.10 A, B, C, we show some smaller oily bubbles with some fluorite particles attached. As the bubbles flow through, the particles attached do not show a favour

on which position of the bubble. In contrast, the particles attached on bigger bubbles are usually concentrated at the front of the bubble. When the oily bubbles are small enough, they flow at the same velocity as the surrounding water phase, the shear stress exhibits on the particles are negligible, the particles are free to move around. However, situations for the bigger ones are different. When the bubbles are huge as the ones shown in Figure 6.10D, E, F, they occupy a large portion of the cross-section area, and the water phase are forced to flow on the sides. The particles in the slurry shows a clear streamline, around the bubbles. When water flow faster than the bubble, it creates a low-pressure zone at the front of the oily bubble. The oil cap if can be seen, and captured particles are more favourable to stay here. In Figure 6.10F, there is no particles observed at the front or any sides of the oily bubble. However, there are particles inside the bubble. These particles are at the bottom of the channel, when the oily bubbles pass through, these particles move along, which indicates they are attached to the bubble. A detailed example of how these particles move is shown below. In Figure 6.10C, the two oily bubbles are attached to each other with particles as the connector. With higher concentration of particles in the slurry, the froth should be more stable as particles acting as a stabilizer as in Pickering emulsion. It is more suitable for these oily bubbles to work in industrial level, since in laboratory, we still need to observe these phenomena.

Figure 6.11 shows how some particles behave around the bubble. Because of the density difference, the particle tends to fall to the lower level in a horizontal flowing channel especially when the front is fully loaded. A particle was at the bottom of a bubble at 0 ms, and when the bubble flowed through at 4 ms, the particle was picked up and flow along the bubble-water interface, to the front of the bubble at 8 ms. Because the front is fully loaded in this case, the particle was pushed down to the bottom of the bubble again, starting another cycle. This phenomenon makes it harder to quantify the particles attached onto a specific bubble, because the particles are moving instead of staying in the same place on a bubble. Also, with the thin channel we fabricated, it is very common for the particles to obstruct the inlet

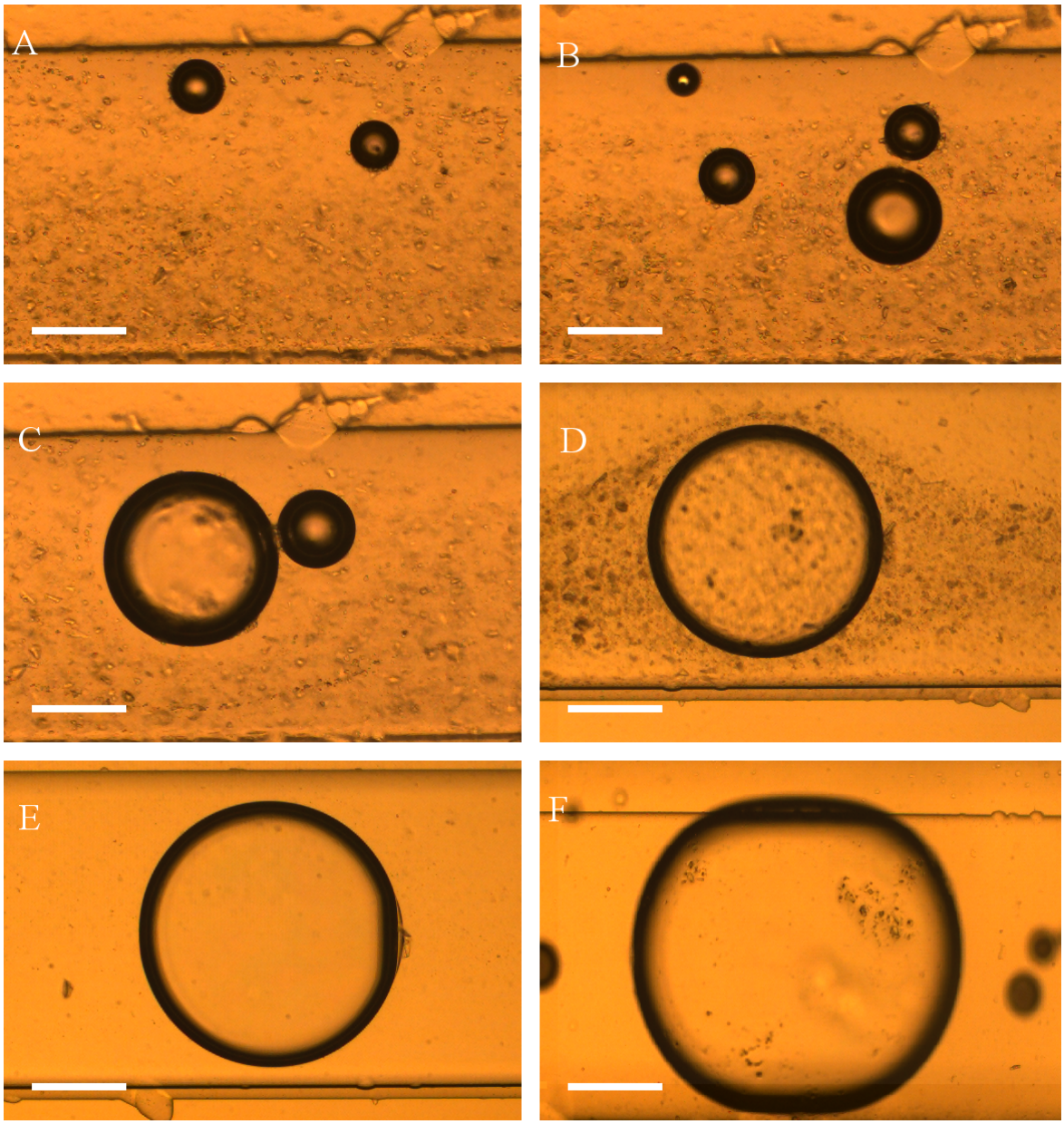

Figure 6.10: Examples of particle-loaded reactive oily bubbles. Flow direction is to the right. Scale bars are 200 μm.

of slurry stream, forcing the experiments to shut down. It is hard to reach a steady slurry stream because of the balancing between all the streams. With gas phase involved in a glass microfluidic chip, the fluctuation of the gaseous pressure can not be dissipated like in a softer PDMS chip. Hence, it will affect the overall flow. We observed inconsistence of particle velocity. Overall, repeating this set of experiments with same flowrate conditions for other chemicals/air bubbles is hardly possible.

Comparing between two scenarios we attempted for the oily bubble/particle interaction, it is obvious that inside the microfluidic chip, the oily bubble captures more fluorite particles, indicating its higher collision efficiency. The confined flow within the microfluidic channel forces particle and oily bubble to collide, thus enhancing the collision efficiency and recovery. This finding could be utilized in industry by creating thousands of parallel channels of microfluidic collision chambers and separate them from the later phase separation unit. The channel of the microfluidics is in tens of micrometers, therefore, a sieve to filter out the larger particles is essential. This technique can be specifically used for fine particles only.

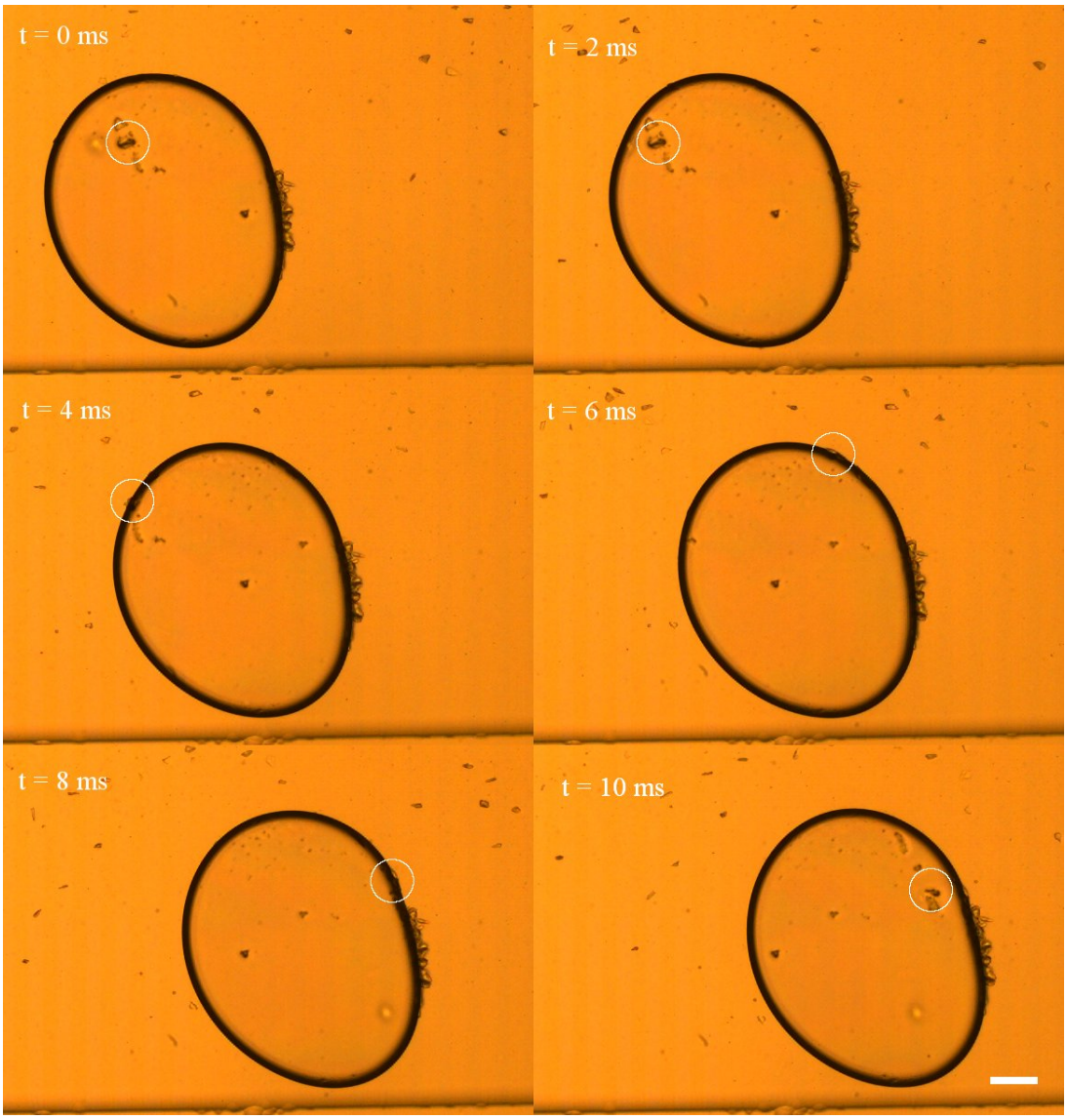

Figure 6.11: Sets of captured images showing how a particle flow along the oily bubble. White circles indicate the same particle. Flow direction is to the right. Scale bar is 100 μm.

7 Conclusion

This dissertation has provided a novel application to the microfluidics and another method to generate reactive oily bubbles. we found out how an unmodified planar PDMS device does not achieve generating oily bubbles. We tested a few designs for the glass devices, and successfully generated reactive oily bubbles. Seven flow patterns were shown by varying flowrate ratios. With high gas and water flowrates with significantly smaller oil flowrate, we have a robust stream of monodispersed oily bubbles. With 20 μm-depth channel, we can generate oily bubbles of around 100 μm with an oil layer of 1 μm at around 100 bubbles per second per channel. We showed captured images of rising oily bubbles with particles attached. We also mix the slurry and the oily bubbles within the microfluidic device. Significant number of particles are shown to attach to the oily bubble. We tried to systematically study the interaction between the oily bubbles and mineral particles, due to the instability of the emulsion and the limited amount, it cannot be fully done. We also compare the loading of mineral particles on the oily bubbles within the channel and in a microflotation cell to show a confined flow system can increase the collision efficiency of fine particles.

8 Future Research

With the parallelization of microfluidic channels, it is possible to achieve the amount required for a gram-level microflotation test. Samples can be collected and weighted like using Hallimond tubes.

The microfluidic device can be used in vertical position, avoiding vertical movement in horizontal setup. With wider channel, it is possible to have every particle attached to be in focus.

With thinner and narrower channels, reactive oily bubbles can be fabricated smaller. In this way, they would be more effective as assisting conventional froth flotation, like small oil droplets or cavitation bubbles.

If we do not have the requirement to present reactive oily bubbles inside the microfluidic channels, the microfluidic pattern can also be simpler. As we shown in the results, when a coflow stream of gas and oil flow into a big reservoir, it is more likely to be broken up into oily bubbles. If the single emulsion is the requirement, parallelization can be much more convenient.

This set up is conveniently adapted for other minerals, because of the monodispersed and easily tuned oily bubbles. If there is a proper method to quantifying the recovery, the study can be done systematically for different size of oily bubbles, different thickness of oil layer, and other factors.

Double emulsions were already used extensively in the field of materials, pharmaceuticals, biological industries, however, there are still areas like wastewater treatment, ion removal which requires liquid-liquid extraction which can utilize the microfluidic generated double emulsions.

References

[1] R. H. Yoon and G. H. Luttrell. The effect of bubble size on fine coal flotation. *Coal Preparation*, 2(3):179–192, 1986.

[2] Roe-Hoan Yoon, Darrin H. Flinn, and Yakov I. Rabinovich. Hydrophobic interactions between dissimilar surfaces. *Journal of Colloid and Interface Science*, 185(2):363 – 370, 1997.

[3] D. Tao. Role of bubble size in flotation of coarse and fine particles—a review. *Separation Science and Technology*, 39(4):741–760, 2005.

[4] M.E Weber and D Paddock. Interceptional and gravitational collision efficiencies for single collectors at intermediate reynolds numbers. *Journal of Colloid and Interface Science*, 94(2):328 – 335, 1983.

[5] Luke Parkinson and John Ralston. Dynamic aspects of small bubble and hydrophilic solid encounters. *Advances in Colloid and Interface Science*, 168(1):198 – 209, 2011. Surface forces and thin liquid films.

[6] D. Feng and C. Aldrich. Effect of particle size on flotation performance of complex sulphide ores. *Minerals Engineering*, 12(7):721 – 731, 1999.

[7] Z.A. Zhou, Zhenghe Xu, J.A. Finch, H. Hu, and S.R. Rao. Role of hydrodynamic cavitation in fine particle flotation. *International Journal of Mineral Processing*, 51(1):139 – 149, 1997. Application of Surface Science to Advancing Flotation Technology.

[8] T.V. Subrahmanyam and K.S.Eric Forssberg. Fine particles processing: shear-flocculation and carrier flotation — a review. *International Journal of Mineral Processing*, 30(3):265 – 286, 1990.

[9] Leonard J Warren. Shear-flocculation of ultrafine scheelite in sodium oleate solutions. *Journal of Colloid and Interface Science*, 50(2):307 – 318, 1975.

[10] Elizaveta Forbes, Dee J. Bradshaw, and George V. Franks. Temperature sensitive polymers as efficient and selective flotation collectors. *Minerals Engineering*, 24(8):772 – 777, 2011.

[11] Mingda Li, Adrien Bussonnière, Matthew Bronson, Zhenghe Xu, and Qingxia Liu. Study of venturi tube geometry on the hydrodynamic cavitation for the generation of microbubbles. *Minerals Engineering*, 132:268 – 274, 2019.

[12] R.-H. Yoon. The role of hydrodynamic and surface forces in bubble–particle interaction. *International Journal of Mineral Processing*, 58(1):129 – 143, 2000.

[13] J. Liu, T. Mak, Z. Zhou, and Z. Xu. Fundamental study of reactive oily-bubble flotation. *Minerals Engineering*, 15(9):667 – 676, 2002.

[14] Yulan Chen, Zhenzhen Lu, and Qingxia Liu. Janus membrane emulsification for facile preparation of hollow microspheres. *Journal of Membrane Science*, 592:117384, 2019.

[15] Vince Wallwork, Zhenghe Xu, and Jacob Masliyah. Bitumen recovery with oily air bubbles. *The Canadian Journal of Chemical Engineering*, 81(5):993–997, 2003.

[16] Li Su, Zhenghe Xu, and Jacob Masliyah. Role of oily bubbles in enhancing bitumen flotation. *Minerals Engineering*, 19(6–8):641 – 650, 2006. Selected papers from the Centenary of Flotation Symposium, 5–9 June 2005, Brisbane, Australia.

[17] Fang Zhou, Louxiang Wang, Zhenghe Xu, Qingxia Liu, and Ruan Chi. Reactive oily bubble technology for flotation of apatite, dolomite and quartz. *International Journal of Mineral Processing*, 134:74 – 81, 2015.

[18] Fang Zhou, Louxiang Wang, Zhenghe Xu, Yaoyang Ruan, and Ruan Chi. A study on novel reactive oily bubble technology enhanced collophane flotation. *International Journal of Mineral Processing*, 169:85 – 90, 2017.

[19] M.J. Mankosa, J.N. Kohmuench, L. Christodoulou, and E.S. Yan. Improving fine particle flotation using the stackcell™ (raising the tail of the elephant curve). *Minerals Engineering*, 121:83 – 89, 2018.

[20] Todd Thorsen, Richard W. Roberts, Frances H. Arnold, and Stephen R. Quake. Dynamic pattern formation in a vesicle-generating microfluidic device. *Phys. Rev. Lett.*, 86:4163–4166, Apr 2001.

[21] Alfonso M. Gañán Calvo. Generation of steady liquid microthreads and micron-sized monodisperse sprays in gas streams. *Phys. Rev. Lett.*, 80:285–288, Jan 1998.

[22] Paul J. A. Kenis, Rustem F. Ismagilov, and George M. Whitesides. Microfabrication inside capillaries using multiphase laminar flow patterning. *Science*, 285(5424):83–85, 1999.

[23] Thomas Cubaud and Thomas G. Mason. Capillary threads and viscous droplets in square microchannels. *Physics of Fluids*, 20(5):053302, 2008.

[24] Shingo Okushima, Takasi Nisisako, Toru Torii, and Toshiro Higuchi. Controlled production of monodisperse double emulsions by two-step droplet breakup in microfluidic devices. *Langmuir*, 20(23):9905–9908, 2004. PMID: 15518471.

[25] Zhihong Nie, Shengqing Xu, Minseok Seo, Patrick C. Lewis, and Eugenia Kumacheva. Polymer particles with various shapes and morphologies produced in continuous microflu-

idic reactors. *Journal of the American Chemical Society*, 127(22):8058–8063, 2005. PMID: 15926830.

[26] Assaf Rotem, Adam R. Abate, Andrew S. Utada, Volkert Van Steijn, and David A. Weitz. Drop formation in non-planar microfluidic devices. *Lab Chip*, 12:4263–4268, 2012.

[27] Tuan M. Tran, Sean Cater, and Adam R. Abate. Coaxial flow focusing in poly(dimethylsiloxane) microfluidic devices. *Biomicrofluidics*, 8(1):016502, 2014.

[28] S. Torza and S. G. Mason. Coalescence of two immiscible liquid drops. *Science*, 163(3869):813–814, 1969.

[29] Jan Guzowski, Piotr M. Korczyk, Slawomir Jakiela, and Piotr Garstecki. The structure and stability of multiple micro-droplets. *Soft Matter*, 8:7269–7278, 2012.

[30] Jiandi Wan, Alexander Bick, Matthew Sullivan, and Howard A. Stone. Controllable microfluidic production of microbubbles in water-in-oil emulsions and the formation of porous microparticles. *Advanced Materials*, 20(17):3314–3318, 2008.

[31] Heon-Ho Jeong, Sagar Yadavali, David Issadore, and Daeyeon Lee. Liter-scale production of uniform gas bubbles via parallelization of flow-focusing generators. *Lab Chip*, 17:2667–2673, 2017.

[32] Heon-Ho Jeong, Zhuo Chen, Sagar Yadavali, Jianhong Xu, David Issadore, and Daeyeon Lee. Large-scale production of compound bubbles using parallelized microfluidics for efficient extraction of metal ions. *Lab. Chip*, 19:665–673, 2019.

[33] M. L. Eggersdorfer, W. Zheng, S. Nawar, C. Mercandetti, A. Ofner, I. Leibacher, S. Koehler, and D. A. Weitz. Tandem emulsification for high-throughput production of double emulsions. *Lab Chip*, 17:936–942, 2017.

Appendix

Detailed Procedure for the Fabrication of Glass Microfluidic Chip

Clean the Substrate with Piranha Solution

900 mL sulfuric acid (H_2SO_4, 96%) and 300 mL hydrogen peroxide (H_2O_2, 30%) are mixed inside a square container to create piranha solution. The substrates are loaded on a Teflon carrier and immersed inside the piranha bath for 15 minutes. Then the substrates are rinsed with large amount of water to remove the piranha solution and dried with nitrogen gun for further use. This process can remove organic substance on the substrate by oxidizing and dissolving them in the solution.

Sputtering of Chrome and Gold layer

The cleaned substrate was put in high vacuum at 10^{-7} Torr and sputtered 20 nm of chrome and 150 nm of gold for the protection for HF etching in further steps. This process was done in an automated planar DC magnetron sputtering system.

Spincoating of Photoresist

The photoresist to use in this case is HPR 504 which is a very common positive photoresist used in micromachining. The photoresist was coated on the gold side of the substrate on a spin coater at 4000 rpm to achieve a uniform 1.25 μm film. The substrate was then baked at 115 °C for 90 seconds. The substrate was then placed on a mask aligner and covered by patterned photomask. The substrate was then flooded by UV light. Unlike negative photoresist like SU-8, HPR 504 becomes soluble in the developer after UV light exposure. After exposure, the substrate was immersed in 354 developer for 30 seconds and rinsed in water for 90 seconds. If there are defects on the photoresist, it is easily removable by acetone

and isopropanol with or without UV exposure and redo the coating process again.

Metal Etching

Before this part of process, the substrate has a uniform stage of glass with uniform films of chrome and gold with patterned HPR 504. the substrate was then immersed in gold etchant, a mixture of potassium iodide, iodine and water, for 50 seconds. The etching process can be seen by eyes that the gold faded into chrome. The substrate was then rinsed by water and immersed in chrome etchant, a mixture of ceric ammonium nitrate, nitric acid and water, for 20 seconds. The etching process can be seen by eyes that the chrome faded. After chrome etching, the substrate was rinsed by water and immersed in gold etchant for 2 seconds to remove chrome oxide formed on the glass surface. Then the substrate was rinsed by water and dried by nitrogen gun.

Glass Etching

Before this part of process, the substrate has a uniform stage of glass with patterned HPR 504, gold and chrome. The depth created by the missing pattern of photoresist and metal layers is measured as a reference before etching, which is usually around 1.4 μm. Then a blue tape was used to cover the back side of the glass substrate to eliminate unwanted etching on the other side. The substrate was then loaded on a Teflon carrier and placed in a plastic container with the presence of borofloat etchant. It was taken out of the solution after 5 minutes and rinsed by large amount of water and dried. Then the depth was measured again. The etching rate can be calculated with this method. The rest of the etching process can be precisely timed to achieve precise depth of channel. Because the etching is homogeneous, the etching process happened in every direction. The aspect ratio (width/depth) will always be larger than 2.

Removal of Remaining Photoresist and Metal Layers

After the HF etching had been finished, the substrate was rinsed by acetone followed by isopropanol and water to remove the remaining photoresist. Then the metal layers were removed like in the metal etching process but with longer time to fully remove the remaining metal. The substrate would be inspected under the microscope for any metal leftover since a clean substrate is essential for the next step, glass bonding.

Port Drilling

A blank borofloat glass wafer is aligned with patterned substrate and inlet and outlet ports are marked in the blank substrate. Holes of 1.7 mm in diameter were drilled on the wafer for inlet and outlet ports using Servo Precision Drill Press.

Glass Bonding

The patterned substrate and drilled wafer were cleaned with piranha solution as the steps stated above. Then they are cleaned by soap solution to remove any dust and leftover. The two wafers are aligned under a microscope and bonding by pressing with hands. Any gaps between the substrate can be seen as interference pattern. Until now, the bonded glass were still separable by knife and redo this bonding process. After they were temporarily bonded by above steps, the device can be heated in a Muffle furnace at 600 °C for two hours for annealing of the glass to achieve permanent bonding between the wafers.

MATLAB Files

preliminary.m

```
% find all the folders containing the original pictures
try
    a = folderSearch(cd, 'cihx'); %PFV 4 files
```

```
catch
    a = folderSearch(cd, 'cih'); %PFV 3 files
end

num_of_sets = numel(a.folder);
fprintf('Start of preminary processing, there are overall %d sets of data to
     process. \n', num_of_sets)
temp_new_switch = 1; %change to 1 to save greyscale images


if 0 % change to 1 if images require cropping
    xy_list = zeros(num_of_sets, 4);
    for j = 1:num_of_sets

        folder = char(a.folder(j));
        name = char(a.name(j));
        name = name(1:length(name) - 5);
        cd(folder)
        filename = sprintf(strcat(name, '%06d.tif'), 1);
        imshow(im2double(rgb2gray(imread(filename))) * 16);
        [x, y] = ginput(2);
        xy_list(j, 1:4) = [x', y'];
        cd('..')
    end
end

for j = 1:num_of_sets

    folder = char(a.folder(j));
    name = char(a.name(j));
    name = name(1:length(name) - 5);
    %make folders
    if temp_new_switch
        mkdir(strcat(name, '_temp_new'))
    end
    mkdir(strcat(name, '_diff'))

    cd(folder)
    c = dir('*.tif');
    num_of_pics = numel(c);
    temp = cell(num_of_pics,1);
    temp_new = cell(num_of_pics,1);
    diff = cell(num_of_pics, 1);

    for i = 1:num_of_pics
```

```
    filename = sprintf(strcat(name,'%06d.tif'),i);
    temp{i} = rgb2gray(imread(filename));
    try
        temp_new{i} = temp{i,1}(floor(xy_list(j,3)):floor(xy_list(j,4)),
            floor(xy_list(j,1)):floor(xy_list(j,2)));
    catch
        temp_new{i} = temp{i,1};
    end
end

%size of the new graphs
[x, y] = size(temp_new{1,1});

% find background
avg = zeros(x,y);
for i = 1:num_of_pics
    avg = avg + im2double(temp_new{i, 1}) * 16;
end
avg = avg/num_of_pics;

%process diff
max_mat = zeros(num_of_pics, 1);
for i = 1:num_of_pics
    diff{i,1} = avg - im2double(temp_new{i,1}) * 16;
    max_mat(i,1) = max(max(diff{i,1}));
end
overall_max = max(max_mat);
for i = 1:num_of_pics
    diff{i,1} = diff{i,1} / overall_max;
end


%save pics to temp_new and diff
if temp_new_switch
    cd(strcat('..\',name,'_temp_new'))
    for i = 1:num_of_pics
        imwrite(uint8(temp_new{i,1}),sprintf(strcat(name,'_temp_new_%04d.
            png'),i))
    end
end
if 1
    cd(strcat('..\',name,'_diff'))
    for i = 1:num_of_pics
        imwrite(uint8((diff{i,1})*255),sprintf(strcat(name,'_diff_%04d.png
            '),i))
```

```
        end
        cd ..
    end
    %display current set
    disp(j)
end
disp('End of preminary processing.')
beep
```

folderSearch.m

```
% DataToProcessAddress = 'C:\Users\vitalii.dodonov\Desktop\2017.09.01\White
    Sparger\5LPM\circulation 1';
% ext = 'mat';
function FileList = folderSearch(DataToProcessAddress, ext)
MATLABfunctionAddress = cd;
paths = subFolderPaths(DataToProcessAddress);
level = 1;
pathsTotal{level, 1} = DataToProcessAddress;
level = 2;
pathsTotal{level, 1} = paths;
%%
while ~isempty(pathsTotal{level, 1})
    level = level + 1;
    nPaths = size(pathsTotal{end, 1} ,1);
    pathTemp = [];
    for i = 1:nPaths
        pathTemp = [pathTemp; subFolderPaths(pathsTotal{level-1, 1}{i})];
        pathsTotal{level, 1} = pathTemp;
    end
end
%%
extension = ['*.', ext];
FileList.folder = {};
FileList.name = {};
FileList.full = {};
for i = 1:size(pathsTotal, 1)
    pathsBatch = pathsTotal{i};
    for j = 1:size(pathsBatch, 1)
        if ~ischar(pathsBatch)
            Address = pathsBatch{j, 1};
        else
            Address = pathsBatch;
        end
        cd(Address);
        FilesFoundArray = dir(extension);
```

```
        cd(MATLABfunctionAddress);
        for k = 1:size(FilesFoundArray, 1)
            FileList.folder = [FileList.folder; Address];
            FileList.name = [FileList.name; FilesFoundArray(k).name];
            FileList.full = [FileList.full; sprintf('%s\\%s', Address,
                FilesFoundArray(k).name)];
        end
    end
end
end
```

subFolderPaths.m

```
% Checks what is in the input directory and outputs a list of full paths of
% of subfolders
function paths = subFolderPaths(directory)
paths = [];
d = dir(directory);
d(~[d.isdir]) = []; %remove non-directories
d(ismember({d.name}, {'.', '..'})) = []; %% Remove hidden directories . and
    ..
if ~isempty(d) > 0;
    nameFolds = {d.name}';
    for i = 1:size(nameFolds, 1);
        paths{i, 1} = [directory, '\', nameFolds{i}];
    end
end
```

displacement.m

```
date = 'F12';
%load('displa.mat')
displacement_mat = zeros(85,1);
for series = 85
    cd(sprintf('%s_S%02d_diff_%s', date, series, 'b'))
    no_of_pics = numel(dir('*.png'));
    cd ..

    bubble_prop_mat = [];

    for pics = 1:no_of_pics
        bubble_pics = imread(sprintf('%s_S%02d_diff_%s/%s_S%02d_diff_%s_%04d.
            png', date, series, 'b', date, series, 'b', pics));
        index_bubble = [];
        [B_b, L_b, N_b, A_b] = bwboundaries(bubble_pics);
        no_pattern_b = numel(B_b);
```

```
    no_bubble = 0;

    bubble_prop_mat_single = [];
    for pattern = 1:no_pattern_b
        temp = find(L_b == pattern);
        if bubble_pics(temp(1)) == 0
            inner = find(A_b(:,pattern));
            for j = inner'
                index_bubble = [index_bubble; j, pattern];
                no_bubble = no_bubble + 1;
            end
        end
    end

    %record all bubble
    for i = 1:no_bubble
        [bubble_in_x, bubble_in_y] = find(L_b == index_bubble(i,1));
        %pattern for inner of bubble(white)

        bubble_prop = [pics, ...            %1  no of pics
                    index_bubble(i,:), ... %2,3 pattern in | pattern out
                    mean(bubble_in_x), ...  %4  mean x
                    mean(bubble_in_y), ...  %5  mean y
                    numel(bubble_in_y), ...   %6  inner area
                    numel(find(L_b == index_bubble(i,2))), ... %7 outer
                        area
                    0, ...                  %8  eqv y
                    0];                     %9  no of bubble


        bubble_prop_mat_single = [bubble_prop_mat_single; bubble_prop];
    end
    bubble_prop_mat = [bubble_prop_mat; bubble_prop_mat_single];
end
    button = 1;
    bubble_x_list = [];
    bubble_y_list = [];
    beep

    for pics = bubble_prop_mat(1,1):bubble_prop_mat(1,1)+50
        if button < 3
            cd(sprintf('%s_S%02d_diff_%s', date, series, 'b'))
            bubble_pics = imread(sprintf('%s_S%02d_diff_%s_%04d.png', date
                , series, 'b', pics));
            cd ..
```

```
            [B, L, N, A] = bwboundaries(bubble_pics);
            imshow(bubble_pics)
            title(strcat(num2str(series),'-',num2str(pics)))

            [x, y, button] = ginput(1);
            close all
            if button < 2
                number = find(bubble_prop_mat(:,2) == L(floor(y), floor(x))
                    & bubble_prop_mat(:,1) == pics);
                bubble_x_list = [bubble_x_list, bubble_prop_mat(number, 4)
                    ];
                bubble_y_list = [bubble_y_list, bubble_prop_mat(number, 5)
                    ];
            end
        end
    end


    displacement_y = mean(bubble_y_list(2:end) - bubble_y_list(1:end-1));
    displacement_mat(series) = displacement_y;
end

save('displa.mat', 'displacement_mat');
```

count_ step_ v3.m

```
date = 'G29';
tic
load('displa.mat');
    %for series = [121:144,31,32,43,44,49,51:53,65:67,69]
    for series = [40:47, 49:57, 59,60,62,63]
        %clearvars

        %series
        cd(sprintf('%s_S%02d_diff_%s', date, series, 'o'))
        no_of_pics = numel(dir('*.png'));
        cd ..
        bubble_prop_mat = [];
        oil_prop_mat = [];
        oily_bubble_prop_mat = [];
        drop_prop_mat = [];

        for pics = 1:no_of_pics
            bubble_pics = imread(sprintf('%s_S%02d_diff_%s/%s_S%02d_diff_%s_
                %04d.png', date, series, 'b', date, series, 'b', pics));
            bubble_pics = ~bwareaopen(~bwareaopen(bubble_pics,20),20);
```

```
oil_pics = imread(sprintf('%s_S%02d_diff_%s/%s_S%02d_diff_%s_%04d.
    png', date, series, 'o', date, series, 'o', pics));

[oil_pics_x, oil_pics_y] = find(oil_pics == 0);
for i = 1:size(oil_pics_x,1)
    x_1 = max(oil_pics_x(i) - 1,1);
    x_2 = min(oil_pics_x(i) + 1, size(oil_pics,1));
    y_1 = max(oil_pics_y(i) - 1,1);
    y_2 = min(oil_pics_y(i) + 1, size(oil_pics,2));
    oil_pics(x_1, y_1) = 0;
    oil_pics(x_1, oil_pics_y(i)) = 0;
    oil_pics(x_1, y_2) = 0;
    oil_pics(oil_pics_x(i), y_1) = 0;
    oil_pics(oil_pics_x(i), y_2) = 0;
    oil_pics(x_2, y_1) = 0;
    oil_pics(x_2, oil_pics_y(i)) = 0;
    oil_pics(x_2, y_2) = 0;

end
if 0
    oil_pics = [ones(size(oil_pics,1),1), oil_pics,ones(size(
        oil_pics,1),1)];
    %add a white border on the left and right border of the oil
        pics to avoid
end
index_bubble = [];
index_oil = [];

[B_b, L_b, N_b, A_b] = bwboundaries(bubble_pics);
[B_o, L_o, N_o, A_o] = bwboundaries(oil_pics);
[B_bb, L_bb, N_bb, A_bb] = bwboundaries(bubble_pics'); %transpose
    bubble pics
cleared_oil_pics = bwareaopen(oil_pics, 600);

no_pattern_b = numel(B_b);
no_pattern_o = numel(B_o);

no_bubble = 0;
no_drop = 0;
no_oily_bubble = 0;

bubble_prop_mat_single = [];
oil_prop_mat_single = [];
oily_bubble_prop_mat_single = [];
drop_prop_mat_single = [];
```

```
for pattern = 1:no_pattern_b
    temp = find(L_b == pattern);
    if bubble_pics(temp(1)) == 0
        inner = find(A_b(:,pattern));
        for j = inner'
            try
                [sharp_points, position] = find_sharp_points(B_b{j},
                    15);

                if isempty(sharp_points)
                    index_bubble = [index_bubble; j, pattern];
                    no_bubble = no_bubble + 1;
                end
            catch
                index_bubble = [index_bubble; j, pattern];
                no_bubble = no_bubble + 1;
            end
        end
    end
end

%record all bubble
for i = 1:no_bubble
    [bubble_in_x, bubble_in_y] = find(L_b == index_bubble(i,1));
    %pattern for inner of bubble(white)

    bubble_prop = [pics, ...            %1  no of pics
                index_bubble(i,:), ... %2,3 pattern in | pattern
                    out
                mean(bubble_in_x), ...  %4  mean x
                mean(bubble_in_y), ...  %5  mean y
                numel(bubble_in_y), ...   %6  inner area
                numel(find(L_b == index_bubble(i,2))), ... %7
                    outer area
                0, ...                  %8  eqv y
                0];                     %9  no of bubble
    if L_b(floor(bubble_prop(4)),floor(bubble_prop(5))) ~=
        bubble_prop(2)
```

```
        bubble_prop(4) = mean(bubble_in_x(1:floor(bubble_prop(6)/2)
            ));
        bubble_prop(5) = mean(bubble_in_y(1:floor(bubble_prop(6)/2)
            ));
        if L_b(floor(bubble_prop(4)),floor(bubble_prop(5))) ~=
            bubble_prop(2)
            [bubble_in_y1, bubble_in_x1] = find(L_bb == L_bb(
                bubble_in_y(1), bubble_in_x(1)));
            bubble_prop(4) = mean(bubble_in_x1(1:floor(bubble_prop
                (6)/2)));
            bubble_prop(5) = mean(bubble_in_y1(1:floor(bubble_prop
                (6)/2)));
            if L_b(floor(bubble_prop(4)),floor(bubble_prop(5))) ~=
                bubble_prop(2)
                [bubble_in_y1, bubble_in_x1] = find(L_bb == L_bb(
                    bubble_in_y(1), bubble_in_x(1)));
                bubble_prop(4) = mean(bubble_in_x1(floor(bubble_prop
                    (6)/2):end));
                bubble_prop(5) = mean(bubble_in_y1(floor(bubble_prop
                    (6)/2):end));
            end
        end
    end

    bubble_prop_mat_single = [bubble_prop_mat_single; bubble_prop
        ];
end


for pattern = 1:no_pattern_o
    temp = find(L_o == pattern);
    if oil_pics(temp(1)) == 0
        inner = find(A_o(:, pattern));
        for j = inner'
            index_oil = [index_oil; j, pattern];
            no_drop = no_drop + 1;
        end
    end
end

%check double surrounding
double_sur = [];
try
    for oil_pat = [index_oil(:,2)]'
        temp = find(A_o(oil_pat, :));
```

```
        if temp ~= 1
            temp1 = find(A_o(temp,:));
            if ~isempty(temp1)
                double_sur = [double_sur; index_oil(index_oil(:,2)
                    == oil_pat,:), temp];
            end
        end
    end
catch
end


%record all oil
for i = 1:no_drop
    if numel(find(L_o == index_oil(i,1))) > 600
        [oil_in_x, oil_in_y] = find(L_o == index_oil(i,1)); %
            pattern for inner of bubble(white)

        oil_prop = [pics, ...          %1  no of pics
                    index_oil(i,:), ... %2,3 pattern in | pattern
                        out
                    mean(oil_in_x), ...  %4  mean x
                    mean(oil_in_y), ...  %5  mean y
                    numel(oil_in_y),...    %6  inner area
                    0];                  %7  whether on a side

        oil_prop_mat_single = [oil_prop_mat_single; oil_prop];
    end
end
no_drop = size(oil_prop_mat_single,1);

%if no_bubble && no_drop
if no_drop
    for i = 1:no_bubble
        try
            temp = find(oil_prop_mat_single(:,2) == L_o(floor(
                bubble_prop_mat_single(i, 4)), floor(
                bubble_prop_mat_single(i, 5))));
            % find the pattern in oil_pic for the bubbles in
                bubble_pic
        catch
            temp = [];
        end

        if ~isempty(temp)
```

```
        no_oily_bubble = no_oily_bubble + 1;
        oily_bubble_prop = [bubble_prop_mat_single(i, :),... %
            1-9 bubble properties
                        oil_prop_mat_single(temp, 2:3),... %
                            10-11 bubble in the oil pics
                        i,temp,...              %12-13 index of
                            bubble in bubble pics and oil pics
                        0,... % 14 area for oil area
                        0,... %15 area for oil border area
                        0]; %16

        oily_bubble_prop_mat_single = [
            oily_bubble_prop_mat_single; oily_bubble_prop];
    end

end

for j = 1:size(double_sur,1)

    bubble_inside = oily_bubble_prop_mat_single(
        oily_bubble_prop_mat_single(:,11) == double_sur(j,1),:);
    oil_prop_mat_single(oil_prop_mat_single(:,3) == double_sur(
        j,3),7) = double_sur(j,1);
end

for j = unique(oil_prop_mat_single(:,3))'
    count_indv_bub_drop = 0;
    try
        bubbles_inside = oily_bubble_prop_mat_single(
            oily_bubble_prop_mat_single(:,11) == j,:);
    catch
        bubbles_inside = [];
    end
    for i = oil_prop_mat_single(oil_prop_mat_single(:,3) == j,
        2)'
        [sharp_points, position] = find_sharp_points(B_o{i}, 15)
            ;
        if isempty(sharp_points) || isempty(bubbles_inside)
            count_indv_bub_drop = count_indv_bub_drop + 1;
        else
            bubble_attached_p = zeros(size(sharp_points,1),1);
            for k = 1:size(sharp_points,1)
                min_min_dis = zeros(size(bubbles_inside,1),1);
                for lm = 1:size(bubbles_inside,1)
                    min_dis = 1e5;
```

```
                list_bub_border = B_o{bubbles_inside(lm,10)
                    ,1};
                for n = 1:size(list_bub_border,1)
                    min_dis = min(min_dis, distance_p(
                        sharp_points(k,:), list_bub_border(n
                        ,:)));
                end
                min_min_dis(lm) = min_dis;
            end
            if min(min_min_dis) < 25
                if numel(bubbles_inside(min_min_dis == min(
                    min_min_dis),10)) > 1
                    temp = bubbles_inside(min_min_dis == min(
                        min_min_dis),10);
                    bubble_attached_p(k) = temp(1);
                else
                    bubble_attached_p(k) = bubbles_inside(
                        min_min_dis == min(min_min_dis),10);
                end
            end
        end
        oil_prop_mat_single(oil_prop_mat_single(:,3) == j &
            oil_prop_mat_single(:,2) == i,7) = mode(
            bubble_attached_p);
    end
end

if count_indv_bub_drop > 1
    M = watershed(bwdist(cleared_oil_pics));


    list_indv_bub_drop = find(oil_prop_mat_single(:,3) == j
        & oil_prop_mat_single(:, 7) == 0);
    current = zeros(count_indv_bub_drop,2);
    border_ratio = [];
    for i = 1:count_indv_bub_drop
        %main
        %find the region in watershed for individual
        %bubble/drop
        region = M(floor(oil_prop_mat_single(
            list_indv_bub_drop(i),4)),floor(
            oil_prop_mat_single(list_indv_bub_drop(i),5)));

        %find the region in watershed for other oil in the
            same
```

```
    %bubble
    oil_area = 0;
    for k = find(oil_prop_mat_single(:,7) ==
        oil_prop_mat_single(list_indv_bub_drop(i),2))'

        [temp1, temp2] = find(L_o == oil_prop_mat_single(
            k,2));
        region = [region,M(temp1(1),temp2(1))];
        oil_area = oil_area + oil_prop_mat_single(k,6);
    end




    try
        %find the bubble in the individual bubble/drop
        temp = find(oily_bubble_prop_mat_single(:,13) ==
            list_indv_bub_drop(i));
    catch
        temp = [];
    end
    if isempty(temp)
        %single droplet
        drop_prop_mat_single = [drop_prop_mat_single;[
            oil_prop_mat_single(list_indv_bub_drop(i),:)
            ,0,0]];
        current(i,:) = [size(drop_prop_mat_single,1), 0];

    else
        oily_bubble_prop_mat_single(temp,14) = oil_area;
        %find the oil border for this oily bubble/droplet
        current(i,:) = [temp, 1];

    end
    oily_bubble_border = numel(find(L_o ==
        oil_prop_mat_single(list_indv_bub_drop(i),3) &
        ismember(M,region)));

    border_ratio(i) = oily_bubble_border;


end
overall_border = numel(find(L_o == oil_prop_mat_single(
    list_indv_bub_drop(i),3)));
```

```
        actual_border_ratio = overall_border/sum(border_ratio).*
            border_ratio;
        for i = 1:count_indv_bub_drop
            if current(i,2) == 1
                oily_bubble_prop_mat_single(current(i,1), 15) =
                    actual_border_ratio(i);
            else
                drop_prop_mat_single(current(i,1), 7) =
                    actual_border_ratio(i);
            end
        end

    else
        if ~isempty(bubbles_inside)
            oil_area = 0;
            for k = find(oil_prop_mat_single(:,3) == j &
                oil_prop_mat_single(:,2) ~= bubbles_inside(1,10))
                '
                oil_area = oil_area + oil_prop_mat_single(k,6);
            end
            oily_bubble_prop_mat_single(
                oily_bubble_prop_mat_single(:,11) == j,14) =
                oil_area;
            oily_bubble_border = numel(find(L_o ==
                bubbles_inside(1,11)));
            oily_bubble_prop_mat_single(
                oily_bubble_prop_mat_single(:,11) == j,15) =
                oily_bubble_border;
        else

            drop_prop_mat_single = [drop_prop_mat_single;[
                oil_prop_mat_single(oil_prop_mat_single(:,3) == j
                ,:),0,0]];
            drop_prop_mat_single(end,7) = numel(find(L_o ==
                drop_prop_mat_single(end,3)));
        end

    end
end


for j = 1:size(double_sur,1)
    try
    bubble_inside = oily_bubble_prop_mat_single(
        oily_bubble_prop_mat_single(:,10) == double_sur(j,1),:);
```

```
                oil_prop_mat_single(oil_prop_mat_single(:,3) == double_sur(
                    j,3),7) = double_sur(j,1);

                oily_bubble_prop_mat_single(oily_bubble_prop_mat_single
                    (:,10) == double_sur(j,1),[14,15]) = ...
                    [drop_prop_mat_single(drop_prop_mat_single(:,2) ==
                        double_sur(j,3),6), ...
                    drop_prop_mat_single(drop_prop_mat_single(:,2) ==
                        double_sur(j,3),7) + oily_bubble_prop_mat_single(
                        oily_bubble_prop_mat_single(:,10) == double_sur(j,1)
                        ,7)];
                drop_prop_mat_single(drop_prop_mat_single(:,2) ==
                    double_sur(j,3),:) = [];
                catch
                end
            end


        end

        oily_bubble_prop_mat = [oily_bubble_prop_mat;
            oily_bubble_prop_mat_single];
        bubble_prop_mat = [bubble_prop_mat; bubble_prop_mat_single];
        oil_prop_mat = [oil_prop_mat; oil_prop_mat_single];
        drop_prop_mat = [drop_prop_mat; drop_prop_mat_single];
    end
%       %%
    %calculate movement of bubble


    displacement_y = displacement_mat(series);
    bubble_prop_mat(:,8) = bubble_prop_mat(:,5) - bubble_prop_mat(:,1) *
        displacement_y;
    try
        drop_prop_mat(:,8) = drop_prop_mat(:,5) - drop_prop_mat(:,1) *
            displacement_y;
    end
    num_of_ind_bubble = 0;
    num_of_ind_droplet = 0;

    for i = 1:size(bubble_prop_mat,1)
        if bubble_prop_mat(i,1) == 1
            num_of_ind_bubble = num_of_ind_bubble + 1;
            bubble_prop_mat(i,9) = num_of_ind_bubble;
        else
```

```
        temp = find((bubble_prop_mat(:,1) - bubble_prop_mat(i,1)) > -4
            &...
                   (bubble_prop_mat(:,1) - bubble_prop_mat(i,1)) < 0
                      &...
                  abs(bubble_prop_mat(:,8) - bubble_prop_mat(i,8)) <
                      50 &...
                  abs(bubble_prop_mat(:,4) - bubble_prop_mat(i,4)) <
                      50 &...
                  abs((bubble_prop_mat(:,6) - bubble_prop_mat(i,6))/
                      bubble_prop_mat(i,6)) < 0.15);
        if isempty(temp)
            num_of_ind_bubble = num_of_ind_bubble + 1;
            bubble_prop_mat(i,9) = num_of_ind_bubble;
        else
            bubble_prop_mat(i,9) = bubble_prop_mat(temp(1),9);
        end
    end
end

for i = 1:size(drop_prop_mat,1)
    if drop_prop_mat(i,1) == 1
        num_of_ind_droplet = num_of_ind_droplet + 1;
        drop_prop_mat(i,9) = num_of_ind_droplet;
    else
        temp = find((drop_prop_mat(:,1) - drop_prop_mat(i,1)) > -4
            &...
                   (drop_prop_mat(:,1) - drop_prop_mat(i,1)) < 0 &...
                  abs(drop_prop_mat(:,8) - drop_prop_mat(i,8)) < 50
                      &...
                  abs(drop_prop_mat(:,4) - drop_prop_mat(i,4)) < 50
                      &...
                  abs((drop_prop_mat(:,6) - drop_prop_mat(i,6))/
                      drop_prop_mat(i,6)) < 0.15);
        if isempty(temp)
            num_of_ind_droplet = num_of_ind_droplet + 1;
            drop_prop_mat(i,9) = num_of_ind_droplet;
        else
            drop_prop_mat(i,9) = drop_prop_mat(temp(1),9);
        end
    end
end

%oily_bubble_prop_mat = oily_bubble_prop_mat(2:end,:);
%oil_prop_mat = oil_prop_mat(2:end,:);
for i = 1:size(oily_bubble_prop_mat,1)
```

```
            oily_bubble_prop_mat(i,16) = bubble_prop_mat(bubble_prop_mat(:,1)
                == oily_bubble_prop_mat(i,1) & bubble_prop_mat(:,2) ==
                oily_bubble_prop_mat(i,2) ,9);
        end
%         %%
        %output
        if 1
            mkdir(sprintf('%s_S%02d_diff_%s', date, series, 'n'))
            for pics = 1:no_of_pics
                cd(sprintf('%s_S%02d_diff_%s', date, series, 'o'))
                oil_pics = imread(sprintf('%s_S%02d_diff_%s_%04d.png', date,
                    series, 'o', pics));
                cd ..
                imshow(oil_pics)
                title(strcat(num2str(series),'-',num2str(pics)))
                temp = find(oily_bubble_prop_mat(:,1) == pics);
                for i = temp'
                    text(oily_bubble_prop_mat(i, 5), oily_bubble_prop_mat(i, 4)
                        , num2str(oily_bubble_prop_mat(i, 16)))
                end
                if ~isempty(drop_prop_mat)
                    temp = find(drop_prop_mat(:,1) == pics);
                    for i = temp'
                        text(drop_prop_mat(i, 5), drop_prop_mat(i, 4), num2str(
                            drop_prop_mat(i, 9)),'Color','red')
                    end
                end
                pause(0.05)
                cd(sprintf('%s_S%02d_diff_%s', date, series, 'n'))
                saveas(gcf, sprintf('%s_S%02d_diff_%s_%04d.png', date, series,
                     'n', pics))
                cd ..
            end
        end

        if 1
            final_drop_list = [];
            if ~isempty(drop_prop_mat)
                num_of_indv_droplet = 0;
                for i = [unique(drop_prop_mat(:,9))]'
                    num_of_indv_droplet = num_of_indv_droplet + 1;
                    temp = find(drop_prop_mat(:,9) == i);
                    %if numel(temp) > 1 && bubble_prop_mat(temp(1),5) < 500
                    final_drop_list = [final_drop_list;[num_of_indv_droplet,
                        mean(drop_prop_mat(temp,6)),mean(drop_prop_mat(temp,7))
```

```
                    ]];

                end
            end

            final_bubble_list = [];
            num_of_indv_bubble = 0;
            for i = [unique(oily_bubble_prop_mat(:,16))]'
                num_of_indv_bubble = num_of_indv_bubble + 1;
                temp = find(oily_bubble_prop_mat(:,16) == i);
                final_bubble_list = [final_bubble_list;...
                                     [num_of_indv_bubble,...
                                      oily_bubble_prop_mat(temp(1),16),...
                                      mean(oily_bubble_prop_mat(temp,6)),...
                                      mean(oily_bubble_prop_mat(temp,7)),...
                                      mean(oily_bubble_prop_mat(temp,14)),...
                                      mean(oily_bubble_prop_mat(temp,15))]];
            end

            try
                drop_prop_mat = sortrows(drop_prop_mat,9);
            catch
            end
            try
                oily_bubble_prop_mat = sortrows(oily_bubble_prop_mat,16);
            catch
            end

            csvwrite(sprintf('%s_S%02d_final_droplet.csv', date, series),
                final_drop_list)
            csvwrite(sprintf('%s_S%02d_final_bubble.csv', date, series),
                final_bubble_list)
            csvwrite(sprintf('%s_S%02d_all_droplet.csv', date, series),
                drop_prop_mat)
            csvwrite(sprintf('%s_S%02d_all_bubble.csv', date, series),
                oily_bubble_prop_mat)
            save(sprintf('%s_S%02d.mat', date, series), 'oily_bubble_prop_mat'
                , 'bubble_prop_mat', 'oil_prop_mat', 'drop_prop_mat')
        end

    toc
    end
beep
```

find_ sharp_ points.m

```
function [sharp_points, position] = find_sharp_points(list_border, distance)
    %border is a list of coordinates 2 by n of the border in coutner
    %clockwise direction
    sharp_points = [];
    no_point = size(list_border, 1);
    position = [];

    for P2_index = 1:no_point
        P1_index = P2_index - distance;
        if P1_index < 1
            P1_index = P1_index + no_point;
        end

        P3_index = P2_index + distance;
        if P3_index > no_point
            P3_index = P3_index - no_point;
        end

        P1 = list_border(P1_index,:);
        P2 = list_border(P2_index,:);
        P3 = list_border(P3_index,:);

        cross_product = cross([P2(2) - P1(2),...
                               P2(1) - P1(1),0],...
                              [P3(2) - P2(2),...
                               P3(1) - P2(1),0]);

        angle = acos(dot(P2-P1, P2-P3)/norm(P2-P1)/norm(P2-P3))/pi()*180;

        if angle < 80
            sharp_points = [sharp_points; P2];
            position = [position; P2_index];
        end
    end
end
```

distance_ p.m

```
function l = distance_p(pos1, pos2)
    l = sqrt((pos1(1) - pos2(1))^2 + (pos1(2)-pos2(2))^2);
end
```